Na-Cl Cotransporter (*SLC12A3*) Inhibition Exacerbates Age-Related Macular Degeneration Via the Nrf2/HO-1 Ferroptosis Pathway

Chengming Chen,[1,2] Tingke Xie,[1] Huan Zhang,[3] Lifu Chang,[1] Yanyan Lan,[4] Chao Fan,[1] Dongyu Wei,[5] Xiaolan Wang,[1] Sida Liu,[1] Yixuan Chen,[1] Yuhao Chen,[1] Xuejiao Wang,[6] Xiaolong Yan,[6] Lei Shang,[7] Liyuan Tao,[8] and Jing Han[1]

[1]Department of Ophthalmology, Tangdu Hospital, The Fourth Military Medical University, Xi'an, China
[2]Department of Ophthalmology, The 900th Hospital of Joint Logistic Support Force, PLA (Fuzong Clinical Medical College of Fujian Medical University), Fuzhou, China
[3]Department of Gastroenterology, Air Force Medical Center, The Fourth Military Medical University, Beijing, China
[4]College of Rehabilitation Medicine, Fujian University of Traditional Chinese Medicine, Fuzhou, China
[5]Center of Clinical Aerospace Medicine, The Fourth Military Medical University, Xi'an, China
[6]Department of Thoracic Surgery, Tangdu Hospital, The Fourth Military Medical University, Xi'an, China
[7]Department of Health Statistics, School of Preventive Medicine, The Air Force Military Medical University, Xi'an, China
[8]Research Center of Clinical Epidemiology, Peking University Third Hospital, Beijing, China

Correspondence: Jing Han, Department of Ophthalmology, Tangdu Hospital, The Fourth Military Medical University, 569 Xinsi Rd., Xi'an 710038, China; hanjing.cn@163.com.
Liyuan Tao, Research Center of Clinical Epidemiology, Peking University Third Hospital, 49 North Garden Rd., Haidian District, Beijing 100191, China; tendytly@163.com.
Lei Shang, Department of Health Statistics, School of Preventive Medicine, The Air Force Military Medical University, 169 Changle West Rd., Xi'an 710038, China; shanglei@fmmu.edu.cn.

CC, TX, HZ, and LC contributed equally to the work presented here and should therefore be regarded as equivalent authors.

Received: January 28, 2025
Accepted: July 12, 2025
Published: September 10, 2025

Citation: Chen C, Xie T, Zhang H, et al. Na-Cl cotransporter (*SLC12A3*) inhibition exacerbates age-related macular degeneration via the Nrf2/HO-1 ferroptosis pathway. *Invest Ophthalmol Vis Sci.* 2025;66(12):24. https://doi.org/10.1167/iovs.66.12.24

Purpose. To explore the causal links between antihypertension drugs usage and age-related macular degeneration (AMD).

Methods. Multiple genetic analyses, including summary data-based Mendelian randomization (SMR), traditional MR, and colocalization analysis, were used to explore the causal associations between antihypertension drugs and AMD. Clinical data from the UK Biobank and the National Health and Nutrition Examination Survey (NHANES) was applied to refined risk assessment of specific antihypertensive medications in the context of AMD development. In vitro and in vivo oxidative stress models, mediated by $NaIO_3$, were utilized to study the impact of specific antihypertensive drugs and target genes on AMD pathogenesis.

Results. Genetic analyses substantiated the causal relationship between increased *SLC12A3* expression and a lowered AMD risk. Colocalization analysis supported the shared causal attributes between *SLC12A3* expression and AMD. Cross-sectional analysis results based on UK Biobank indicated that AMD risk was significantly lower in participants taking thiazide diuretics with other antihypertensives or not on antihypertensives compared to those on thiazides alone. The results based on NHANES support the above results. In vivo and in vitro experiments showed that thiazide diuretics worsened retinal damage in AMD mouse models, and *SLC12A3* knockdown disrupted the balance of oxidative stress in retinal pigment epithelium (RPE) cells. Further molecular mechanism experiments showed that *SLC12A3* knockdown promoted retinal degeneration by regulating RPE ferroptosis through activation of the Nrf2/HO-1 pathway.

Conclusions. Our study underscores a notable causal association between thiazide diuretic use and AMD risk and reveals a potential mechanism by which inhibition or downregulation of *SLC12A3* (sodium–chloride cotransporter [NCC]) contributes to AMD progression. However, deeper exploration is needed to enhance the accuracy and validity of our findings.

Keywords: age-related macular degeneration, Na-Cl cotransporter, *SLC12A3*, thiazides diuretics, ferroptosis

The aging population makes organ degeneration a global health concern, and the vision loss in the elderly caused by age-related macular degeneration (AMD) is severely impacting the quality of life for patients worldwide.[1] By 2040, the global population affected by AMD will soar to 288 million.[2] Based on the Beckmann international classification criteria for AMD and the AMD staging criteria proposed by the Age-Related Eye Disease Study (AREDS) group, AMD is predominantly categorized into three distinct stages: early AMD, intermediate AMD, and advanced AMD.[3,4]

The retinal changes in dry-AMD patients (80%–90% of the total number of AMD patients) are mainly manifested as drusen, retinal pigment epithelium changes, and map-like atrophy, whereas the retinal change in wet-AMD patients is primarily neovascularization.[5] The progression of AMD is influenced by a multifaceted interplay of factors including age, ethnicity, and genetics. Moreover, systemic conditions such as high blood pressure have been recognized as significant contributors to AMD risk,[2,6,7] primarily through their adverse effects on the functionality of the retinal blood vessels.[8]

Considering the detrimental impact of hypertension on AMD, antihypertensive therapy is of theoretical importance for improving AMD prognosis.[9] Nonetheless, the efficacy of various antihypertensive medications in treating AMD remains a topic of debate. Findings from a randomized controlled trial indicate that calcium channel blocker usage poses a risk factor for AMD.[10] The results of a 20-year longitudinal observational study linked oral β-blocker usage significantly with the risk of developing wet AMD.[11] By aggregating data from three cohort studies, an increased risk of early-stage AMD was found to be associated with β-blocker use, although no connection to advanced AMD was found.[12] In contrast, a cohort study, the California Teachers Study, identified a significant association between the use of antihypertensive drugs and an elevated risk of AMD, particularly highlighting an increased risk associated with diuretics compared to other antihypertensive medications.[13] Another case–control study showed that thiazide diuretic intake was positively associated with severe vision loss and extensive choroidal neovascularization with severe subretinal hemorrhage.[14] Notably, given the limitations of the limited number and quality of the samples included, as well as the inherent inability of the observational design to fully eliminate confounding factor influences, no current observational study evidence has conclusively established a causal link between antihypertensive drug use and the various subtypes of AMD.

Mendelian randomization (MR) analysis stands out as a powerful genetic statistical technique that leverages the principles of Mendel's second law using single nucleotide polymorphisms (SNPs) as instrumental variables (IVs). MR analyses are less susceptible to confounders, and SNPs used are often drawn from large-scale genome-wide association study (GWAS) databases.[15–17] In parallel, Bayesian colocalization analysis provides a probabilistic framework to assess shared causal attributes between exposure and outcome variables, offering a nuanced understanding of their interrelation.[18] By integrating MR and colocalization analyses, we aimed to pinpoint potential causal relationships between genetic proxies of various antihypertensive drugs and AMD. To enhance the robustness and applicability of our findings, we corroborated the genetic analysis results with clinical data from the UK Biobank and the National Health and Nutrition Examination Survey (NHANES). We also used a sodium iodate ($NaIO_3$)–induced AMD model, a classical AMD model that can cause local oxidative stress and retinal pigment epithelium (RPE) damage, to conduct in vitro and in vivo mechanistic studies.[19] Our aim was to deliver a refined risk assessment of specific antihypertensive medications in the context of AMD development, bridging the gap between genetic insights and clinical implications.

Materials and Methods

Data Sources of Genetic Analyses and Cross-Sectional Study

Because racial differences can heavily bias the results of MR analyses, all SNPs employed for genetic analysis were sourced from GWAS databases focused exclusively on individuals of European ancestry.[20] Our study utilized expression quantitative trait loci studies (eQTLs) as proxies for specific antihypertensive drug targets, reflecting the expression levels of drug target RNA, and this part of the data was obtained from the eQTLGen Consortium, with a sample size of 31,684 participants.[21] For AMD GWAS data, we relied on FinnGen data freeze 9, which included 8913 cases and 348,936 controls.[22] A portion of the data originated from a meta-analysis conducted by Winkler and colleagues,[23] which was incorporated into the IEU OpenGWAS project. This dataset contained information regarding patients in the early phase of AMD, with a total of 14,034 cases and 91,214 controls. All early AMD diagnoses within this dataset were verified through color fundus photography.[23] GWAS data for dry AMD (sample size: 6065 cases and 251,042 controls) and wet AMD (sample size: 4848 cases and 252,277 controls), which were defined as advanced AMD, also was obtained from FinnGen data freeze 9. In the FinnGen database, the diagnostic categorization of AMD relies on the International Classification of Diseases, 10 Revision (ICD-10; code H35.3) and ICD-9 (code 362.5). GWAS data related to systolic blood pressure (SBP), used in positive control analyses, were derived from a comprehensive meta-analysis incorporating data from the International Consortium for Blood Pressure and the UK Biobank, totaling a sample size of 757,601.[24] The distinct sources of IVs for exposure and outcome variables across different databases ensured that there was no sample overlap in our MR analysis. Cross-sectional study data were obtained from the UK Biobank and two cycles of the NHANES spanning the years 2005 to 2008, with a sample size of 20,482. The UK Biobank is a large demographic cohort with phenotypic, genomic, proteomic, and metabolomic data from more than 500,000 participants.[25] NHANES is a cross-sectional clinical study conducted by the U.S. National Center for Health Statistics, drawing on extensive interview data from a broad population base, and this dataset included comprehensive demographic, laboratory, and questionnaire results. Further details on the GWAS data sources are available in Supplementary Table S1, facilitating transparency and reproducibility of our findings.

Genetic Analyses Design and SNP Extraction

The target genes of antihypertensive drugs commonly used in clinical practice—angiotensin-converting enzyme inhibitors, β-blockers, angiotensin II receptor antagonists (ARBs), calcium channel blockers, potassium-sparing diuretics, aldosterone antagonists, and thiazide diuretics—were identified by consulting the DrugBank database (the included genes and their descriptions are presented in Supplementary Table S2). Based on previous research,[26] the summary data-based MR (SMR) method was applied to screen out the drug targets potentially associated with AMD. Using SNPs in the blood significantly related to the gene proxies of the above-mentioned antihypertensive drug targets based on specific screening criteria (minor allele frequency > 0.01; $P < 5 \times 10^{-8}$), we selected *cis*-eQTLs

within 1 Mb on both sides of the above genes as IVs for SMR.

The inverse variance-weighted MR (IVW-MR) method was utilized to further clarify the causal relationships between AMD and the target genes selected by SMR. The gene window for *cis*-eQTLs was set to within 100 kb of either side of the target gene. The results of weighted median method were used to reinforce the IVW findings. Traditional MR analysis aimed to include a maximal number of strong IVs (linkage disequilibrium analysis: $r^2 < 0.3$; 100 kb; $P < 5 \times 10^{-8}$).[27] Moreover, positive control tests were conducted simultaneously to verify the causal effect of the target genes selected by SMR on SBP to enhance confidence in the MR results. When performing traditional MR analysis, we strictly adhered to the Strengthening the Reporting of Observational Studies in Epidemiology Using Mendelian Randomization (STROBE-MR) guidelines[28]; weak IVs were excluded as defined and detailed in the Supplementary Materials.[29] Because the eQTLs database used lacks AGTR1, one of the major gene proxies of ARB, we would further extract relevant SNPs from previously published studies[30] for MR analysis and present the results in Supplementary Table S3.

Bayesian colocalization analysis was conducted to evaluate the shared causal characteristics between the selected target genes and AMD. The posterior probabilities of five diverse hypotheses were calculated: (1) P(H1), the probability that antihypertensive drug target genes and AMD are not associated; (2) P(H2), the probability associated only with antihypertensive drug target genes; (3) P(H3), the probability associated only with AMD; (4) P(H4), the probability of a correlation between antihypertensive drug target genes and AMD, but with a significant probability of causal variation; and (5) P(H5), the probability that antihypertensive drug target genes and AMD are correlated, and antihypertensive drug target genes and AMD have the same probability of causal variation.[31] The probability that a SNP was independently associated with trait 1 (P_1) and trait 2 (P_2) was set to 1×10^{-4}, and the probability (P_{12}) that a SNP was associated with both trait 1 and trait 2 was set to 1×10^{-5}. P(H4) ≥ 0.8 was considered high-grade colocalization evidence, $0.5 \leq P$(H4) < 0.8 was considered moderate-grade colocalization evidence.[32]

Cross-Sectional Study Design and Participant Inclusion Criteria

In the definition of baseline assessment of AMD status based on the data from UK Biobank, we mainly relied on the ICD-9 and ICD-10 eye disease codes from relevant hospital episode statistical records of participants. The use status of various antihypertensive drugs based on the UK Biobank questionnaire was further extracted (medication codes are shown in Supplementary Table S12). To explore the potential role of thiazide diuretics in AMD, the information collected on thiazide diuretic usage was further divided into "taking thiazide diuretics only," "thiazide diuretics combined with other antihypertensive drugs," "taking other drugs," and "not taking any antihypertensive drugs." Given that thiazide diuretic usage in the NHANES always occurred in conjunction with other antihypertensive medications, a direct comparison of AMD prevalence between users and non-users of thiazide diuretics was not straightforward. To ensure the comparability of the cross-sectional study, participants who were on thiazide diuretics alongside multiple antihypertensive drugs or in combination with a single specific antihypertensive agent—where the sample size was deemed too small—were excluded. Consequently, the analysis based on NHANES concentrated on evaluating the prevalence of AMD among individuals treated with a combination of thiazide diuretics and ARBs versus those on ARBs alone, with the participant screening process depicted in Figure 1B. The initial univariate analysis aimed to provide elementary insight into the association between thiazide diuretic usage and AMD occurrence. To mitigate the potential confounding impact of various risk factors on AMD development, including age, sex, race, education level, poverty income ratio (PIR) for the NHANES, Townsend deprivation index for the UK Biobank, body mass index (BMI), alcohol consumption, smoking status, hypertension, and diabetes mellitus, these variables were incorporated as covariates in the multivariate analysis. Detailed diagnostic criteria for AMD, medication status, and precise definitions of the covariates are provided in the Supplementary Materials.

Animals and Interventions

Eight-week-old male C57BL/6 mice, purchased from and raised in the Animal Test Center of the Air Force Military Medical University, were used for this experiment. The mice had free access to water and standard food. The humidity of the housing environment was maintained between 45% and 65%, and the light/dark cycle was set to 12/12 hours. All procedures were conducted in accordance with the ARVO Statement for the Use of Animals in Ophthalmic and Vision Research and were approved by the Animal Committee of the Fourth Military Medical University (IACUC-20241342). During the experiment, the mice were divided into three groups by employing a random number table method: $NaIO_3$-naïve, $NaIO_3$-10 mg, and $NaIO_3$-30 mg. To induce the AMD model, the mice received an intraperitoneal injection of 2 mL $NaIO_3$ at doses of 10 mg/kg or 30 mg/kg. Following this, each group of mice underwent intravitreal injections. The right eye of each mouse received a single intravitreal injection of PBS-soluble clopamide (35 µg, 1 µL), a commonly used thiazide diuretic, and the left eye received an equal volume of PBS as a control. Four days later, all mice were subjected to follow-up experiments. Some of the mice were placed in a dark room to rule out the phototoxicity of thiazide drugs. To achieve specific knockdown of *SLC12A3* in the RPE layer of mice, we utilized the pAAV-RPE-mCherry-5′mir30a-shRNA-3′mir30a vector purchased from Tsingke Biotech (Beijing, China). Based on previously established protocols, we adjusted the light intensity of the operating environment to an appropriate brightness. Under the guidance of a dissecting microscope, 1 µL of adeno-associated virus serotype 9 (AAV9)/*SLC12A3* (10^{12} genome copies/mL) was injected into the subretinal space of the right eye using a flat-tipped microsyringe. For the control, the AAV9 empty vector viral supernatant was injected into the subretinal space of the left eye. After 28 days, $NaIO_3$ was administered intraperitoneally, and a follow-up experiment was conducted 4 days later. The short hairpin RNA (shRNA) sequences used in this study are detailed in Supplementary Table S15.

Ethics Approval

Because the human data adopted in this study were all publicly available data from the eQTLGen Consortium,

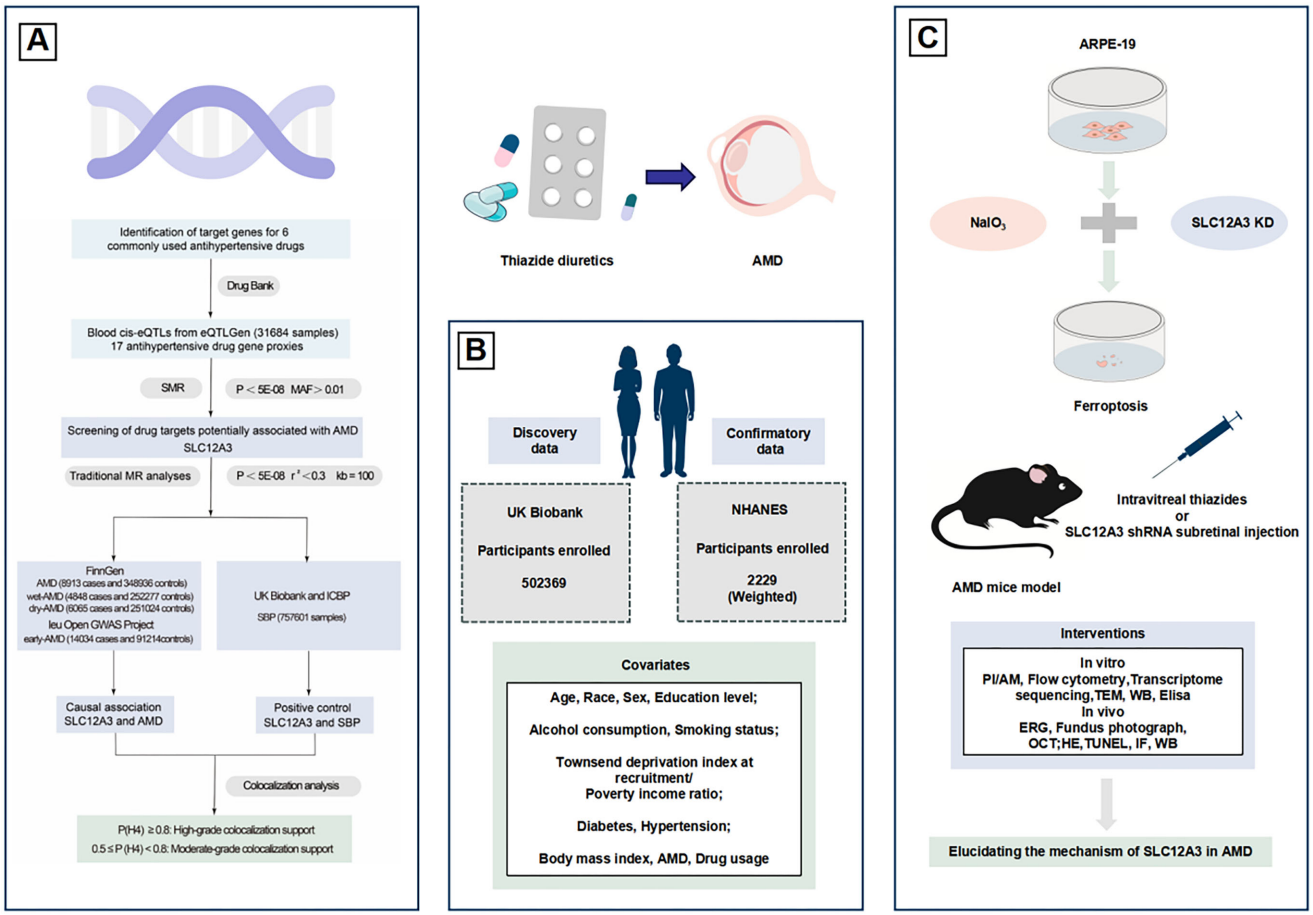

Figure 1. Schematic diagram of study design. (**A**) Genetic analyses workflow. (**B**) Participant screening process for the cross-sectional study. (**C**) Diagram of the in vitro and in vivo tests.

FinnGen database, UK Biobank, IEU OpenGWAS project, and NHANES, all data-related studies were approved by their respective ethical review committees, and written informed consent was provided by the patients. Among them, the clinical data extracted based on the UK Biobank has obtained approval from the North-West Multi-Centre Research Ethics Committee (ref. no. 16/NW/0274; application ID: 784326). Therefore, no additional ethical approval was required for the research portion of this study on humans. All animal research was conducted in accordance with the regulations of the Animal Care and Use Agency Committee.

Electroretinography, Fundus Photography, and Optical Coherence Tomography

In vivo experiments with mice were conducted using electroretinography (ERG; (MonPackONE; Metrovision, Perenchies, France) to evaluate changes in retinal function. Mice were placed in a dark room for 12 hours for dark adaptation before the ERG procedure. Prior to the ERG examination, the mice were kept in the dark overnight and then anesthetized by intraperitoneal injection with 1% sodium pentobarbital solution (3 mL/kg; Sigma-Aldrich, St. Louis, MO, USA). Pupils were dilated using 1% tropicamide. For the ERG recording, the recording electrode was placed in the center of the cornea and the reference electrode on the cheek, and the ground electrode was connected to the tail. The retinal responses to dark adaptation and light adaptation were recorded. Scotopic 0.01 and photopic 3.0 settings were used to assess rod and cone function, respectively, and the average b-wave amplitudes were recorded and statistically analyzed. Immediately following the ERG assessment, a flat color image of the mouse retina was captured using a fundus photographic machine (Rat suit S-50000; Optoprobe, Beijing, China). An OCT scan (isOCT, Optoprobe, UK/Beimen Kun, Toward Pi, CHN) was then performed to obtain clear retinal images centered on the optic nerve. After data collection, topical antibiotics were applied to the ocular surface to prevent infection.

Histological Analysis

After euthanasia of the mice, the eyes were removed and fixed in 4% paraformaldehyde for 24 hours, and the eyeballs were embedded in paraffin. A 6-µm retinal slice was made along the vertical meridian through the optic disc for hematoxylin and eosin (H&E) staining and TUNEL staining. An upright light microscope (Eclipse E100; Nikon, Tokyo, Japan) and a Nikon digital camera control unit (DS-U3) were used to capture H&E-stained images. Nikon upright fluorescence microscopes (Eclipse C1) and Pannoramic MIDI scanners (3DHISTECH, Budapest, Hungary) were also used to capture H&E-stained images. RPE flatmounts and retinal sections were incubated overnight at 4°C with the primary antibody (details provided in Supplementary Table S14).

This was followed by a 2-hour incubation at room temperature with the corresponding secondary antibody. Then, 4′,6-diamidino-2-phenylindole (DAPI) staining was used to visualize nuclei. Immunofluorescence images were acquired using a confocal microscope (FLUOVIEW FV3000; Olympus, Tokyo, Japan).

Transcriptome Sequencing

Total RNA extraction, cDNA library construction, and sequencing of ARPE-19 cells were performed by RNA sequencing technology at Oebiotech (Shanghai, China). Gene-level segments fragments per kilobase of exon per million mapped fragments [FPKM]) of each enzyme were mapped, and significant changes in gene and transcript expression levels were calculated. Differentially expressed genes (DEGs) were determined by using a cutoff of $P < 0.05$ and an absolute value of $\log_2$ fold change greater than or equal to 0.58. Kyoto Encyclopedia of Genes and Genomes (KEGG) enrichment assays and Reactome enrichment assays were used to determine whether the DEGs of each group were significantly enriched in specific functional classes, pathways, or biological processes. All statistical analysis and image generation in this part were carried out on the oecloud platform.

Transmission Electron Microscopy

ARPE-19 cells from each group were collected and prefixed overnight at 4°C in 2.5% glutaraldehyde phosphate buffer (0.1 M, pH 7.4). The samples were then post-fixed in 2% buffered osmium tetroxide, dehydrated through a graded series of ethanol, and embedded in Epon 12 resin (Hexion, Columbus, OH, USA). Ultrathin sections (60-nm thick) were prepared, stained with uranyl acetate and lead citrate, and observed under a transmission electron microscope (TEM).

JC-1 Staining

Cells from each group were incubated with JC-1 dye (2 µg/mL) for 30 minutes. In healthy mitochondria, JC-1 aggregates exhibit red/orange fluorescence (590 nm), whereas in depolarized mitochondria it appears green (530 nm). Fluorescence images were captured using a confocal microscope, and the relative green-to-red JC-1 fluorescence intensity was quantified using ImageJ software (National Institutes of Health, Bethesda, MD, USA).

Malondialdehyde and Reduced Glutathione Level Detection

For the malondialdehyde (MDA) assay, MDA levels were measured using an MDA assay kit (Servicebio, Wuhan, China). Cells (1×10^7) were collected in 200 µL of MDA lysis buffer and homogenized on ice. The homogenate was centrifuged at 13,000*g* for 10 minutes, and the resulting supernatant was used for analysis. The MDA standard, PBS, and test samples were mixed with the MDA detection solution according to the kit protocol. The mixture was incubated in a 95°C water bath for 40 minutes, followed by immediate cooling in an ice bath for 5 minutes. The samples were then centrifuged at 10,000*g* for 10 minutes. Subsequently, 200 µL of the reaction mixture was added to a 96-well plate, and the absorbance at 532 nm was measured using a microplate reader.

For the glutathione (GSH) assay, GSH levels were quantified using a Servicebio GSH Assay Kit. Cells were collected, resuspended in an appropriate buffer (1×10^6 cells in 300–500 µL PBS or normal saline), and homogenized. The homogenate was centrifuged at 10,000*g* for 10 to 15 minutes at 4°C. The supernatant was then mixed with a protein removal reagent in a 1:1 ratio and centrifuged again under the same conditions. The final supernatant was used for analysis. Following the kit protocol, absorbance at 412 nm was measured using a microplate reader. The GSH content was calculated using the standard curve method.

Ferrous Ion Level Measurement

The intracellular ferrous ion levels were measured using FerroOrange (10 µM). After treatment with the test compounds for the specified durations, cells cultured in six-well plates were resuspended in 500 µL of freshly prepared Hank's Balanced Salt Solution (HBSS). The resuspended cells were incubated at 37°C for 20 minutes to assess fluorescence using Invitrogen BODIPY C11 (Thermo Fisher Scientific, Waltham, MA, USA). Simultaneously, cells from 24-well plates were also resuspended in HBSS and stained with FerroOrange for 30 minutes at 37°C. After staining, the cells were washed three times with HBSS. Fluorescence imaging of FerroOrange-stained cells was captured using a confocal microscope (FLUOVIEW FV3000).

Inductively Coupled Plasma–Mass Spectrometry

ARPE-19 cells from each group were seeded into 24-well plates at a density of 1×10^5 cells per well and cultured in Gibco complete RPMI 1640 medium (Thermo Fisher Scientific) for 3 days. The cells were then treated with $NaIO_3$ or an equal volume of PBS for 5, 30, 60, 180, and 360 minutes. At the end of each time point, collected samples were washed three times with PBS, digested with Accutase solution (Zunyan, Nanjing, China) at 37°C/5% CO_2 for 5 minutes. Following digestion, each sample was divided into two aliquots: one half was used to determine protein concentration via a BCA protein assay kit, and the other half was centrifuged at 450*g* for 5 minutes at 4°C. Subsequently, 250 µL of trace-metal–grade 70% nitric acid was added to the pellet, and the tubes were then placed opened in a metal block heating device until the solution turned yellow. Intracellular Na^+ concentrations were normalized to the total protein content of each sample. Before analysis, the solution was equilibrated to ambient temperature and then subjected to detection using an Agilent 7800 inductively coupled plasma mass spectrometer (ICP-MS; Agilent Technologies, Santa Clara, CA, USA). A set of Na^+ standard solutions with gradient concentrations was prepared and quantified to establish a calibration curve. ARPE-19 cell samples were further diluted at a 100-fold ratio prior to analysis. The ICP-MS instrument was optimized under the following tuning parameters: tune mode set to He MS/MS; tuning elements included ^{7}Li, ^{59}Co, ^{89}Y, ^{95}Mo, ^{197}Au, and ^{204}Tl (all at 1 ppb concentration); radiofrequency (RF) power at 1550 W; RF matching at 1.8 V; sampling depth at 10.0 mm; nebulizer gas flow at 1.04 L/min; He carrier flow at 4.0 mL/min; H_2 flow at 0.0 mL/min; octopole bias at 20 V; octopole RF at 200 V; and energy resolution at 5.0 V.

Investigative Ophthalmology & Visual Science

Sodium Level Measurement

Cells were seeded onto confocal dishes and allowed to adhere overnight. For probe labeling, a mixture of SBFI AM indicator dye (4 µM) and 0.08% Pluronic F-127 was prepared in physiological buffer (PBS) at room temperature and applied to the cells. The cells were incubated with the mixture for 40 minutes. Following incubation, the solution was replaced with probe-free physiological buffer (PBS), and the cells were incubated for an additional 40 minutes. Finally, the cells were washed once with physiological buffer, and fluorescence signals of SBFI AM were detected using appropriate excitation and emission wavelengths.

Cell Culture and Intervention

ARPE-19 cells were cultured in Dulbecco's Modified Eagle Medium/Nutrient Mixture F-12 (DMEM/F-12) containing 100 U/mL penicillin, 100 µg/mL streptomycin, and 10% fetal bovine serum at 37°C in a 5% CO_2 atmosphere. The culture medium was refreshed every 2 days before the experiments commenced. Cells were seeded into various culture vessels as follows: 3.2×10^4 cells per well in 96-well plates, 9.5×10^4 cells per well in 48-well plates, 1×10^5 cells per well in 24-well plates, 1×10^6 cells per well in six-well plates, 2.1×10^6 cells per 6-cm culture dish, and 5.5×10^6 cells per 10-cm culture dish. After 1 day, the cells were in good condition and at the appropriate density, and they were then subjected to intervention. Cells were treated with 10-mM/mL $NaIO_3$ and/or clopamide (dissolved in normal saline) for either 6 or 24 hours. Subsequent experiments were conducted under the same culture conditions for all samples.

Lentivirus Infection and Superoxide Dismutase Activity Assay

The lentivirus for knocking down *SLC12A3* expression and the corresponding empty vector lentivirus were obtained from Tsingke Biotech (detailed siRNA sequences are presented in Supplementary Table S16). Transient transfections were performed using Invitrogen Lipofectamine 2000 (11668019; Thermo Fisher Scientific). After 8 hours, the culture medium was replaced with fresh medium, and the cells were incubated overnight. Subsequently, the cells were re-inoculated for further experiments. The superoxide dismutase (SOD) activity was measured in each group using a SOD Activity Assay Kit (Beyotime Biotechnology, Jiangsu, China). The assay was conducted according to the manufacturer's instructions provided with the kit.

Immunofluorescence Staining of ARPE-19 Cells for *SLC12A3*

ARPE-19 cells were seeded onto confocal dishes and allowed to adhere. The cells were fixed with 4% paraformaldehyde for 15 minutes at room temperature, followed by three washes with PBS. After fixation, the cells were incubated in PBS for 10 minutes at room temperature and washed three more times. To block nonspecific binding, cells were incubated with 5% BSA. After blocking, the primary antibody for *SLC12A3* was applied, and the cells were incubated at 4°C for 12 hours. The cells were then washed three times with PBS and incubated with a fluorescent secondary antibody for 1 hour at room temperature in the dark. Following another three washes with PBS, DAPI was added and incubated for 10 minutes, followed by three additional PBS washes. An anti-fade mounting medium was then applied. Fluorescent images of *SLC12A3* staining were captured using confocal microscopy.

Live/Dead Staining, Reactive Oxygen Species Staining, and Flow Cytometry

ARPE-19 cells were seeded in 48-well plates, and cell viability across different treatment groups was assessed using a Live/Dead kit (Beyotime Biotechnology). In this assay, Calcein AM stained live cells green, and propidium iodide stained dead cells red. After staining for 30 minutes with the Live/Dead kit, images were captured using an Olympus inverted fluorescence digital microscope (LX73). Reactive oxygen species (ROS) distribution in the cells was preliminarily determined using ROS staining. Cells were cultured and treated in confocal dishes, the medium was removed, and the cells were washed three times with PBS. They were then incubated with a 2′,7′-dichlorodihydrofluorescein diacetate (DCFH-DA) probe diluted in serum-free medium (final concentration 10 µmol/L) for 30 minutes in a cell culture incubator. After incubation, the cells were washed three times with PBS, and the results of the ROS staining were imaged using confocal microscopy (Olympus FV10i). Flow cytometry was used to further quantify differences in ROS content between groups. Cells were passed through a 40-µm cell strainer and then excited with a 488-nm laser. Detection was carried out using a 525-nm laser emission in the flow cytometer (FC 500; Beckman Coulter, Brea, CA, USA).

Western Blot Analysis

ARPE-19 cells cultured in vitro or RPE cells isolated from mice were lysed using radioimmunoprecipitation assay (RIPA) buffer (P0013C; Beyotime Biotechnology) supplemented with a protease inhibitor (539134-1SET; EMD Millipore, Burlington, MA, USA). Protein concentrations were determined with the BCA Protein Assay Kit (23225; Thermo Fisher Scientific). Proteins were separated by SDS-PAGE and transferred to polyvinylidene fluoride membranes (ISEQ00010; EMD Millipore). The membranes were blocked with 5% BSA and then incubated with the primary antibodies listed in Supplementary Table S14. After incubation with primary antibodies, the membranes were treated with horseradish peroxidase–conjugated secondary antibodies (rabbit, ZB-2301; mouse, ZB-2305; ZSGB-Bio, Beijing, China). Protein signals were detected using the ECL Plus Western Blot Detection Kit (WBKLS0500; EMD Millipore). Chemiluminescent signals were visualized using a chemiluminescence imaging instrument (Tanon 5200; Tanon, Shanghai, China) and analyzed with ImageJ software.

Wound Healing Assay

We used a marker pen to draw two vertical lines evenly at the bottom of each well in a six-well plate. Cell suspensions were prepared, and cells were counted. Based on the cell counting results, 4×10^5 cells were suspended in 2 mL of medium and added to each well of the six-well plate. The next day, when cell confluence reached 90%, a 200-µL pipette tip was used to draw lines perpendicular to the marked lines on the six-well plate, creating scratches. Floating cells and cell clusters were

Investigative Ophthalmology & Visual Science

gently washed away, and the medium was replaced with serum-free culture medium. This initial scratch distance was considered the 0-hour time point. Two duplicate wells were set for each group, and the experiment was repeated three times. The six-well plate was placed in a cell culture incubator, and images of the scratches were captured at 0 hours and 24 hours. The width of the scratches was measured to calculate the healing rate of each group of cells.

Statistical Analysis

All statistical analyses were executed using R 4.3.2 (R Foundation for Statistical Computing, Vienna, Austria), SMR 1.3.1, SPSS Statistics 23.0 (IBM, Chicago, IL, USA), Prism 8 (GraphPad, Boston, MA, USA), Origin 2021 (OriginLab, Northampton, MA, USA), and FlowJo 10.8.1. To ensure the robustness and validity of our findings, a series of sensitivity analyses was performed: The heterogeneity in dependent instruments (HEIDI) test was employed within the SMR framework to assess linkage disequilibrium between eQTLs and AMD subtypes ($P < 0.01$ was considered pleiotropic).[33] Cochran's Q test and the MR-Egger intercept test were applied in traditional MR analyses to detect heterogeneity and pleiotropy, respectively[34,35]; the default model was the fixed-effects IVW, switching to the multiplicative random-effects IVW model in the presence of heterogeneity.[36,37] Leave-one-out analysis and global test of MR-PRESSO were used to assessed the robustness of the traditional MR analysis, identifying influential outliers that could potentially skew the results.[38,39] The Bonferroni correction method was applied to adjust for multiple comparisons, setting the significance threshold at $P < 0.00074$ for SMR (across 17 × 4 tests) and $P < 0.0125$ for IVW (across four tests) for strong significance. Values within the range of $0.00074 \leq P_{SMR} < 0.05$ and $0.0125 \leq P_{IVW} < 0.05$ were considered suggestively significant.[40] For the multiple regression analysis, age, BMI, Townsend deprivation index, and PIR were presented as medians (25%, 75%), and frequencies (percentages) were used for the remaining covariables. Results from the cross-sectional studies were reported as odds ratios (ORs) with 95% confidence intervals (CIs). The values of the NHANES data were further weighted to reflect the broader US population accurately. $P < 0.05$ was deemed statistically significant. Reference groups for each covariate in the multiple regression analysis are detailed in the Supplementary Materials. For in vitro and in vivo experiments, the data were expressed in mean ± SD. Because the number of groups compared in each test was greater than 3, one-way ANOVA was adopted to calculate the outcome and perform post-analyses. $P < 0.05$ was deemed statistically significant.

Results

SNP Selection and Participant Inclusion

Due to discrepancies between the eQTLGen and DrugBank databases (specifically, the omission of certain antihypertensive drug-related target genes in the eQTLGen database), we ultimately identified 17 gene proxies for the six commonly referenced antihypertensive drugs discussed in the Materials and Methods section. Adhering to the pre-established criteria for instrumental variable IV selection, a particular set of SNPs was extracted for both SMR and traditional MR analysis to investigate the potential causal associations between various antihypertensive drug target genes and AMD (Fig. 1A). The SNPs included in the MR analyses were carefully curated to exclude weak IVs, with an F-statistic threshold greater than 10, as detailed in Supplementary Tables S3 to S11. The comprehensive genetic analysis process, including SNP selection and the analytical approach undertaken, is depicted in Figure 1A. After excluding participants who did not meet the inclusion criteria, 502,369 participants from the UK Biobank and 2229 participants from the NHANES were included in this cross-sectional analysis, as illustrated in Figure 1B and Supplementary Figure S1.

Genetic Analyses of Antihypertensive Drug Target Gene Expression With Risks of AMD

The initial phase of our study utilized SMR analysis to examine 17 antihypertensive drug target genes for potential associations with AMD. Notably, our analysis identified the gene *SLC12A3*, which is targeted by thiazide diuretics, as potentially associated with a reduced risk of AMD. The OR from the SMR analysis indicated a significant protective effect ($OR_{SMR} = 0.41$; 95% CI, 0.28–0.60; $P = 4.88E-06$), as detailed in Figure 2. This finding was unique to *SLC12A3*, as no other antihypertensive drug targets demonstrated a potential association with AMD. Subsequent subgroup analyses aligned with the initial results, consistently indicating a potential association between *SLC12A3* expression and a reduced risk across all AMD subtypes. Expanding upon these findings, traditional MR analysis further substantiated the causal relationship between increased *SLC12A3* expression and a lowered AMD risk ($OR_{IVW} = 0.61$; 95% CI, 0.50–0.76; $P = 6.05E-06$), as illustrated in Figure 3. Subgroup analysis based on traditional MR analysis also supported *SLC12A3* as a protective factor for early AMD ($OR_{IVW} = 0.67$; 95% CI, 0.56–0.80; $P = 1.70E-05$), dry AMD ($OR_{IVW} = 0.67$; 95% CI, 0.55–0.83; $P = 2.18E-04$), and wet AMD ($OR_{IVW} = 0.54$; 95% CI, 0.41–0.72; $P = 1.91E-05$). The positive control results further corroborated the detrimental impact of *SLC12A3* expression on SBP (Fig. 3). Additionally, colocalization analysis provided a high degree of evidence supporting the shared causal attributes between *SLC12A3* expression and AMD, including early and wet AMD, with moderate-grade evidence for colocalization with dry AMD (Table 1; Fig. 3).

Association Between Thiazide Diuretic Use and AMD Risk in the UK Population

The baseline data of this cross-sectional study highlighted significant differences across all covariates other than the Townsend deprivation index between AMD patients and those without AMD, as outlined in Table 2. Model 1, a crude model without adjustment for covariates and corresponding to the univariate analysis results, preliminarily suggested a lower risk of AMD among participants taking other antihypertensive drugs compared with those taking thiazide diuretics only. Model 2, a multiple regression model adjusted for age, sex, race, PIR, education level, BMI, smoking and alcohol status, hypertension, and diabetes mellitus, further confirmed that the risk of AMD was significantly reduced in participants who were taking thiazide diuretics combined with other antihypertensive drugs (OR = 0.850; 95% CI, 0.730–0.989; $P = 3.60E-02$) or not taking any antihypertensive drugs (OR = 0.820; 95% CI, 0.715–0.983; $P = 4.00E-03$) compared with those who were taking thiazide diuretics only (Table 3). To further rule out the effect of hypertension

Investigative Ophthalmology & Visual Science

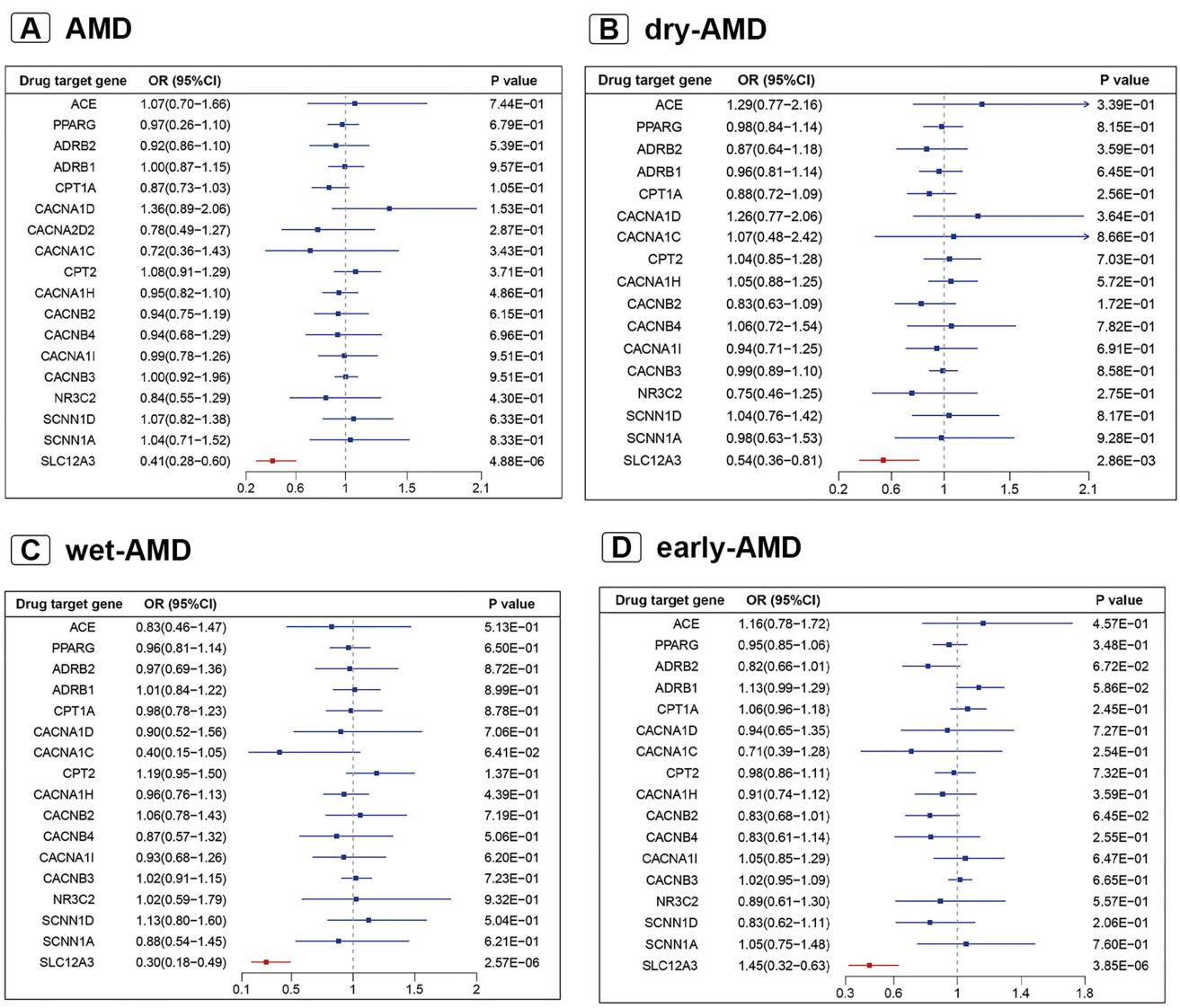

Figure 2. Forest plot of screening out the antihypertensive drug targets potentially associated with AMD via SMR. (**A**) Association between antihypertensive drug target genes and AMD. (**B**) Association between antihypertensive drug target genes and dry AMD. (**C**) Association between antihypertensive drug target genes and wet AMD. (**D**) Association between antihypertensive drug target genes and early AMD.

on AMD itself, model 3, constructed based on model 2 with the additional exclusion of participants with hypertension, was established. Except for the change in Townsend deprivation index, no significant changes occurred in the baseline characteristics of the population in model 3 (Supplementary Table S13). The calculation method of model 2 was then repeated. The outcome of model 3 was consistent with that of model 2, as it also showed that the regimens of taking thiazide diuretics combined with other antihypertensive drugs (OR = 0.785; 95% CI, 0.651–0.946; $P = 1.10E-02$) and not taking any antihypertensive drugs (OR = 0.838; 95% CI, 0.715–0.983; $P = 3.00E-02$) were less harmful for AMD than taking thiazide diuretics only (Table 3).

Thiazide Diuretic Usage and Risk of AMD in the US Population

NHANES data baseline characteristics also indicated that AMD patients and non-AMD patients showed significant differences among all the covariates (Table 4), Model 1, a crude model without adjustment for covariates and corresponding to the univariate analysis, initially suggested that the combination of ARB and thiazide diuretics was a protective factor for AMD compared with ARB alone. Due to the small sample size included, we were unable to further eliminate the participants with hypertension. To enhance the robustness of our analysis, we established two multiple regression models (models 2 and 3) to build on model 1: Model 2 was adjusted for age, sex, race, poverty income ratio, education level, body mass index, and smoking and alcohol status; model 3, based on model 2, was additionally adjusted for hypertension and diabetes mellitus (the two covariates referenced), and the results of model 2 (OR = 1.093; 95% CI, 1.087–1.099; $P < 0.001$) and model 3 (OR = 1.043; 95% CI, 1.038–1.049; $P < 0.001$) both indicated that the combination of ARB and thiazide diuretics, in comparison to using ARB alone, was associated with an increased risk of developing AMD, aligning with the risk observed in the absence of any antihypertensive medication (Table 5).

Investigative Ophthalmology & Visual Science

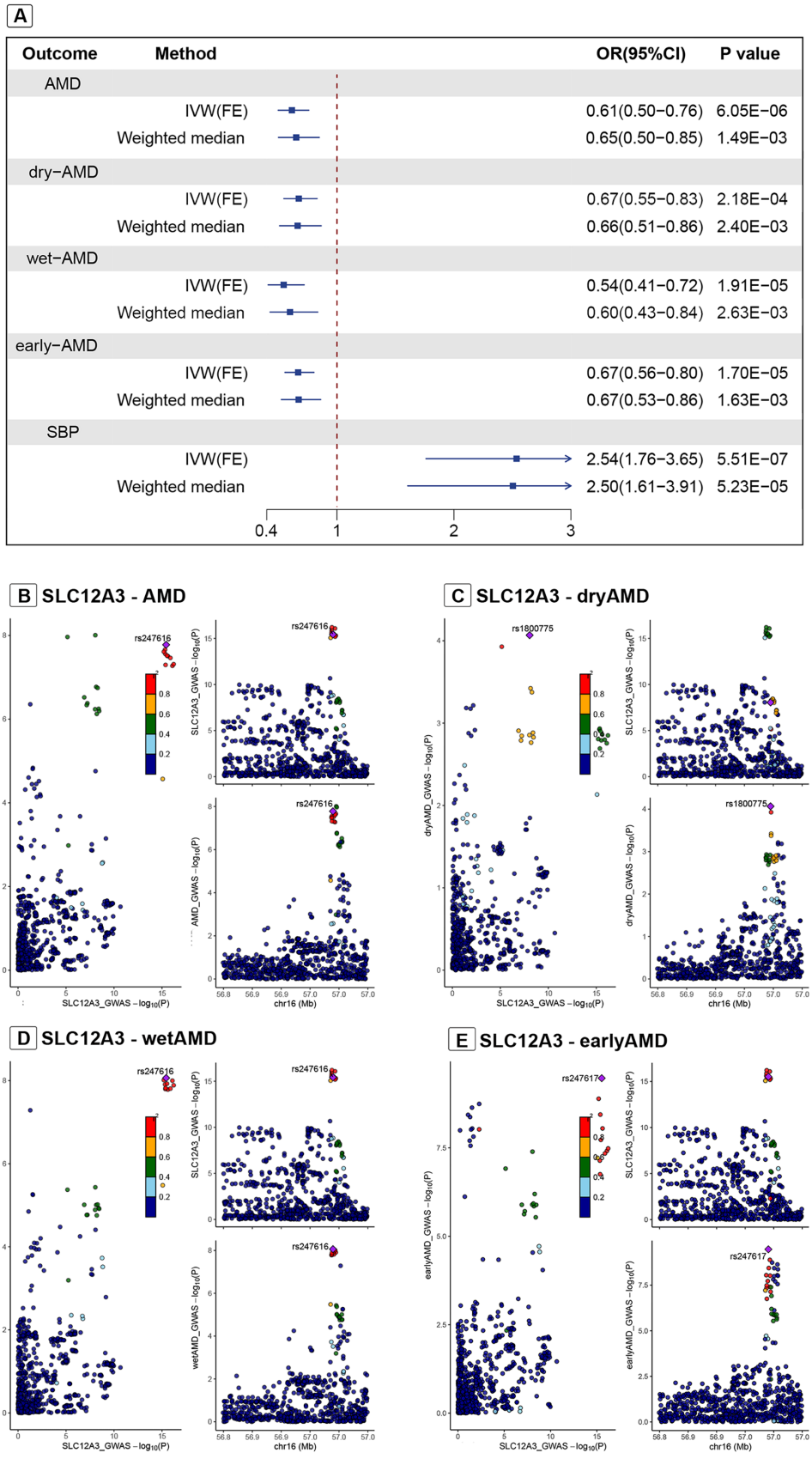

Figure 3. (**A**) Forest plots based on traditional MR illustrating the causal effect of *SLC12A3* expression on AMD and SBP. (**B–E**) LocusCompareR plots depicting colocalization of the lead SNP associated with eQTL of *SLC12A3* and each subtype of AMD. IVW(FE), fixed effects inverse-variance-weighted model.

Table 1. Results of Sensitivity Analysis and Colocalization Analysis for Causal Relations Between *SLC12A3* and Diabetic Retinopathy

Outcome	Eligible *cis*-eQTLs of *SLC12A3*, *n*	SNPs Not Containing Palindromic Sequences or Not Being Outliers, *n*	Cochran's *Q* Test		MR-Egger Intercept Test		MR-PRESSO, *P*, Global Test	HEIDI Test		*P* (H4)
			Q	*P*	Intercept	*P*		*P*	SNPs, *n*	
AMD	87	4	2.13	0.55	−0.019	0.92	0.62	0.11	20	0.98
Dry AMD		5	2.89	0.58	0.08	0.31	0.58	0.54	20	0.57
Wet AMD		4	1.62	0.65	−0.097	0.70	0.70	0.15	20	0.99
Early AMD		4	6.48	0.90	−0.017	0.95	0.19	0.17	20	0.97

Table 2. Baseline Characteristics of the Included UK Participants

Characteristic	Total (*N* = 502369)	Non-AMD (*n* = 488255)	AMD (*n* = 14114)	*P*
Age (y), median (25%, 75%)	58.00 (50.00, 63.00)	58.00 (50.00, 63.00)	63.00 (60.00, 67.00)	<0.001
Sex, *n* (%)				<0.001
Female	273,301 (54.40)	265,104 (54.30)	8,197 (58.10)	
Male	229,068 (45.60)	223,151 (45.70)	5,917 (41.90)	
Race, *n* (%)				<0.001
White	472,573 (94.60)	459,349 (94.60)	13,224 (94.40)	
Mixed	1,923 (0.40)	1,886 (0.40)	37 (0.30)	
Asian or Asian British	9,879 (2.00)	9,528 (2.00)	351 (2.50)	
Black or Black British	9,088 (1.80)	8,837 (1.80)	251 (1.80)	
Chinese	1,573 (0.30)	1,533 (0.30)	40 (0.30)	
Other ethnic group	4,555 (0.90)	4,443 (0.90)	112 (0.80)	
Education level, *n* (%)				<0.001
College or university degree	161,104 (39.60)	157,497 (39.70)	3,607 (35.40)	
A levels/AS levels or equivalent	55,302 (13.60)	54,053 (13.60)	1,249 (12.30)	
0 levels/GCSEs or equivalent	105,170 (25.80)	102,192 (25.80)	2,978 (29.20)	
CSEs or equivalent	26,884 (6.60)	2,6421 (6.70)	463 (4.50)	
NVQ or NHD or NHC or equivalent	32,722 (8.00)	31,744 (8.00)	978 (9.60)	
Other professional qualification	25,798 (6.30)	24,884 (6.30)	914 (9.00)	
BMI (kg/m^2), median (25%, 75%)	26.74 (24.14, 29.91)	26.73 (24.13, 29.89)	27.22 (24.59, 30.57)	<0.001
Townsend deprivation index, median (25%, 75%)	−2.14 (−3.64, 0.55)	−2.23 (−3.64, 0.55)	−2.17 (−3.62, 0.54)	0.76
Hypertension, *n* (%)				<0.001
No	462,258 (92.00)	450,469 (92.30)	11,789 (83.50)	
Yes	40,111 (8.00)	37,786 (7.70)	2,325 (16.50)	
Diabetes mellitus, *n* (%)				<0.001
No	485,768 (96.70)	472,743 (96.80)	13,025 (92.30)	
Yes	16,601 (3.30)	15,512 (3.20)	1,089 (7.70)	
Smoking status, *n* (%)				<0.001
Never	273,449 (54.80)	266,419 (54.90)	7,030 (50.20)	
Previous	173,009 (34.60)	167,267 (34.50)	5,742 (41.00)	
Current	5,2961 (10.60)	51,731 (10.70)	1,230 (8.80)	
Alcohol consumption, *n* (%)				<0.001
Daily or almost daily	101,746 (20.30)	98,711 (20.30)	3,035 (21.60)	
Three or four times a week	115,413 (23.00)	112,511 (23.10)	2,902 (20.60)	
Once or twice a week	129,259 (25.80)	125,996 (25.90)	3,263 (23.20)	
One to three times a month	55,836 (11.10)	54,358 (11.20)	1,478 (10.50)	
Special occasional only	57,989 (11.60)	56,053 (11.50)	1,936 (13.80)	
Never	40,624 (8.10)	39,173 (8.00)	1,451 (10.30)	
Drug usage, *n* (%)				<0.001
Taking thiazide diuretics only	7,172 (1.40)	6,822 (1.40)	350 (2.50)	
Thiazide diuretics combined with other antihypertensive drugs	25,339 (5.00)	24,184 (5.00)	1,155 (8.20)	
Taking other drugs	83,983 (16.70)	80,316 (16.40)	3,667 (26.00)	
Not taking any antihypertensive drugs	385,875 (76.80)	376,933 (77.20)	8,942 (63.40)	

Sensitivity Analysis of Genetic Analyses

HEIDI results for SMR analysis indicated a lack of linkage imbalance between the genetic targets of antihypertensive drugs and AMD, including all subtypes of the condition. In the traditional MR analysis, the results of the MR-Egger intercept test and global test showed that no pleiotropy existed, and the expression of part of IVW was adjusted according to the heterogeneity analysis results based on Cochran's *Q* test. The leave-one-out analysis revealed that the exclusion of any single specific SNP did not significantly alter the overall results (Supplementary Fig. S2), suggest-

Table 3. Association Between Thiazide Diuretic Use and Risk of AMD

	Model 1		Model 2		Model 3	
Thiazide Use Status	**OR (95% CI)**	***P***	**OR (95% CI)**	***P***	**OR (95% CI)**	***P***
Thiazides only	Ref.		Ref.			
Thiazides with other antihypertensive drugs	0.931 (0.824–1.052)	0.252	0.850 (0.730–0.989)	0.036	0.785 (0.651–0.946)	0.011
Other antihypertensive drugs	0.890 (0.795–0.996)	0.042	0.936 (0.814–1.075)	0.349	0.968 (0.820–1.142)	0.697
No drug	1.043 (1.038–1.049)	0.042	0.820 (0.716–0.940)	0.004	0.838 (0.715–0.983	0.030

Model 1 was the crude model without adjustment for covariates. Model 2 was adjusted for age, sex, race, PIR, education level, BMI, smoking and alcohol status, hypertension, and diabetes mellitus. Model 3 was constructed based on model 2, which further excluded participants with hypertension.

Table 4. Baseline Characteristics of the Included US Participants*

Characteristic	**Total (*N* = 2229)**	**Non-AMD (*n* = 2106)**	**AMD (*n* = 123)**	***P***
Age (y), median (25%, 75%)	51.00 (45.00, 59.00)	51.00 (45.00, 58.00)	68.00 (56.00, 79.00)	<0.001
Sex, *n* (%)				<0.001
Female	1046 (47.30)	988 (47.20)	58 (48.20)	
Male	1183 (52.70)	1118 (52.80)	65 (51.80)	
Race, *n* (%)				<0.001
MA	454 (7.800))	435 (7.90)	19 (5.60)	
NHB	508 (11.60))	497 (12.00)	11 (4.60)	
NHW	993 (71.10)	914 (70.70)	79 (80.80)	
OH	197 (4.00)	191 (4.10)	6 (1.90)	
OR	77 (5.50)	69 (5.40)	8 (7.20)	
Education level, *n* (%)				<0.001
Less than 9th grade	343 (7.00)	324 (6.90)	19 (8.30)	
Grades 9–11	348 (11.20)	336 (11.30)	12 (8.30)	
High school graduate/GED or equivalent	549 (26.90)	511 (26.60)	38 (31.80)	
Some college or AA degree	560 (28.20)	524 (28.00)	36 (33.30)	
College graduate or above	428 (26.80)	410 (27.20)	18 (18.20)	
PIR, *n* (%)				<0.001
<1.3	710 (20.20)	667 (20.00)	43 (24.10)	
≥1.3, <3.5	804 (33.40)	755 (33.10)	49 (40.10)	
≥3.5	715 (46.40)	684 (46.90)	31 (35.80)	
BMI (kg/m^2), median (25%, 75%)	27.90 (24.40, 32.00)	27.80 (24.40, 31.90)	29.1 (25.40, 32.30)	<0.001
Alcohol consumption, *n* (%)				<0.001
Never	307 (10.70)	287 (10.50)	20 (12.90)	
Former	472 (18.10)	444 (18.20)	28 (17.20)	
Mild	710 (38.40)	668 (38.30)	42 (41.30)	
Moderate	316 (15.90)	303 (16.00)	13 (12.60)	
Heavy	364 (16.90)	347 (17.00)	17 (16.10)	
Smoking status, *n* (%)				<0.001
Never	1116 (50.50)	1057 (50.80)	59 (44.50)	
Former	585 (24.80)	543 (24.10)	42 (40.80)	
Now	527 (24.60)	505 (25.10)	22 (14.70)	
Hypertension, *n* (%)				<0.001
No	1221 (58.60)	1178 (59.60)	43 (36.10)	
Yes	1007 (41.40)	927 (40.40)	80 (63.90)	
Diabetes mellitus status, *n* (%)				<0.001
Diabetes mellitus	355 (11.00)	338 (11.00)	17 (12.30)	
IFG	131 (5.70)	118 (5.30)	13 (13.10)	
IGT	132 (5.90)	121 (5.60)	11 (12.00)	
No	1606 (77.40)	1524 (78.10)	82 (62.60)	
Drug usage, *n* (%)				<0.001
No	1699 (79.00)	1627 (79.90)	72 (58.00)	
ARB alone	352 (13.60)	314 (12.80)	38 (29.30)	
ARB combined with thiazide diuretics	178 (7.50)	165 (7.00)	13 (12.70)	

AA, associate's degree; BMI, Body mass index; GED, general educational development; IFG, impaired fasting glucose; IGT, impaired glucose tolerance; MA, Mexican American; NHB, non-Hispanic Black; NHW, non-Hispanic White; OH, other Hispanic; OR, other race.

* All results were survey weighted except for counts of categorical variables.

Investigative Ophthalmology & Visual Science

Table 5. Use of ARB and ARB with Thiazide Diuretics and AMD*

Model	ARB Only, OR (95% CI)	ARB With Thiazide Diuretics, OR (95% CI)	No Drug, OR (95% CI)	*P*
1	Ref.	0.769 (0.765–0.773)	0.318 (0.317–0.319)	<0.001
2	Ref.	1.093 (1.087–1.099)	1.257 (1.252–1.263)	<0.001
3	Ref.	1.043 (1.038–1.049)	1.350 (1.344–1.357)	<0.001

Model 1 was the crude model without adjustment for covariates. Model 2 was adjusted for age, sex, race, PIR, education level, BMI, and smoking and alcohol status. Model 3 was adjusted as for model 2, additionally adjusted for hypertension and diabetes mellitus.

* All results were survey weighted except for sample counts.

ing that no individual SNP disproportionately influenced the observed association. All sensitivity analysis results underscored the robustness of our genetic analysis findings (Table 1).

Intravitreal Thiazides Exacerbate Retinal Damage in the $NaIO_3$-Induced Oxidative Stress Mouse Model

To evaluate the role of thiazide diuretics in AMD, we compared retinal phenotypes in mice injected with intravitreal thiazide diuretics versus a placebo. Fundus photography and OCT showed no retinal damage in $NaIO_3$-naïve mice. In contrast, in the $NaIO_3$-10 mg group, thiazide diuretics induced localized RPE layer damage. In the $NaIO_3$-30 mg group, the RPE layers in both eyes appeared "pebbled," with lesions extending to the outer nuclear and inner retinal layers (Figs. 4A, 4B). ERG results indicated no significant difference in light and dark adaptation between eyes treated with thiazide diuretics and those with placebo in the $NaIO_3$-naïve group. However, in the $NaIO_3$-10 mg group, the b-wave amplitude was significantly lower in eyes treated with thiazide diuretics compared to control eyes (Fig. 4C). In the $NaIO_3$-30 mg group, cone and rod cell functions in both eyes were severely disrupted (Supplementary Fig. S3). Histological analysis confirmed these findings: H&E staining showed normal retinal anatomy in the $NaIO_3$-naïve group. In the $NaIO_3$-10 mg group, thiazide diuretics caused significant hypertrophy, atrophy, and depigmentation in the local RPE layer compared to controls. The $NaIO_3$-30 mg group exhibited severe retinal damage, with greater disorder in thiazide-treated eyes, especially in the outer nuclear and inner nuclear layers (Fig. 4D). TUNEL staining further confirmed that thiazide diuretics significantly increased apoptosis in the retinal photoreceptor layer induced by $NaIO_3$ (Fig. 4E). Immunofluorescence staining of zonula occludens-1 (ZO-1) further demonstrated that thiazide diuretics exacerbate the structural damage of RPE cells under oxidative stress conditions (Fig. 4F). In addition, the results of the darkroom group enabled us to cautiously rule out the influence of the phototoxicity of thiazides on the pathological changes observed in our study. By comparing the OCT images and H&E staining results of each group in the darkroom environment, we observed that the "$NaIO_3$-10 mg+CLO" mice showed damage to the RPE layer compared with the "$NaIO_3$-10 mg+PBS" mice, and the damage to all layers of the retina in the "$NaIO_3$-30 mg+CLO" mice was more severe than that in the "$NaIO_3$-30 mg+PBS" mice (Supplementary Figs. S4, S5). The ZO-1 staining results from the darkroom group further corroborated that thiazide diuretics intensify the structural impairment of RPE cells when exposed to oxidative stress (Supplementary Fig. S6). These findings are consistent with the results obtained in the non-darkroom groups.

SLC12A3 Knockdown/Inhibition Exacerbates Oxidative Stress Imbalance and RPE Cell Death When Treated With $NaIO_3$

To investigate the molecular mechanism of thiazide diuretics and their effect on oxidative stress in AMD, we knocked down the target gene *SLC12A3* in ARPE-19 cells and assessed its impact in a $NaIO_3$-induced oxidative stress model. Live/Dead staining showed that $NaIO_3$ increased RPE death, which was further promoted by *SLC12A3* knockdown (Fig. 5A). Focusing on oxidative stress, we observed increased ROS production in cells with *SLC12A3* knockdown. Immunofluorescence staining showed enhanced ROS fluorescence in $NaIO_3$-treated RPE cells, with *SLC12A3* knockdown cells exhibiting the highest fluorescence intensity. Flow cytometry confirmed these results, showing the highest ROS levels in *SLC12A3* knockdown cells (Figs. 5B–E). JC-1 staining results revealed that ARPE-19 cells without $NaIO_3$ treatment exhibited strong red fluorescence, indicating maintenance of mitochondrial membrane potential. However, $NaIO_3$ treatment significantly reduced the red fluorescence and increased the green fluorescence. Moreover, *SLC12A3* knockdown further intensified the green fluorescence, suggesting that *SLC12A3* knockdown exacerbates the disruption of mitochondrial membrane potential under oxidative stress conditions (Fig. 5F). The wound healing assay revealed that $NaIO_3$ significantly impaired the migratory ability of RPE cells, and knockdown of *SLC12A3* further decreased their migration (Fig. 5G). In addition, to more directly verify the effect of thiazide diuretics on RPE cells, we treated the cells with or without 10-mM/mL clopamide for 24 hours and then observed whether the inhibition of sodium–chloride co-transporter (NCC) would exacerbate the RPE damage caused by oxidative stress. The results showed that, compared with the RPE cells in the "Control (Con)+$NaIO_3$" group, the RPE cells in the "Clopamide (CLO)+$NaIO_3$" group exhibited a more significant increase in the mortality rate (Supplementary Fig. S7), levels of ROS (Supplementary Fig. S8), and mitochondrial damage (Supplementary Fig. S9). However, there were no significant differences in the above aspects between the CLO group and the control group.

SLC12A3 Knockdown Promotes Ferroptosis of RPE Cells Treated With $NaIO_3$ by Activating the Nrf2/HO-1 Pathway

To further explore the underlying mechanism of the role of *SLC12A3* in AMD, we first performed immunofluorescence staining of ARPE-19 cells to clarify the spatial

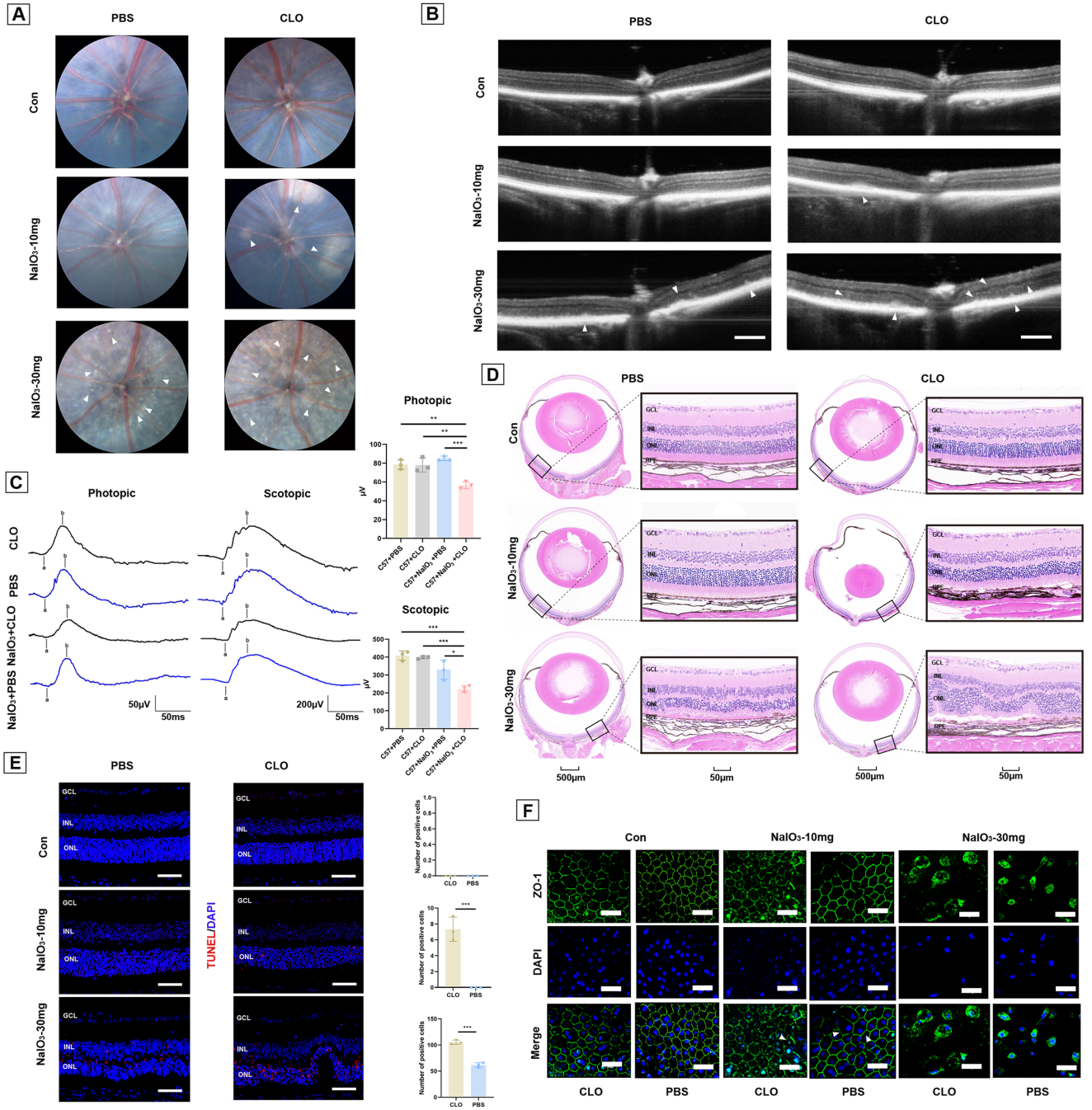

Figure 4. Thiazide diuretics exacerbates retinal damage in the $NaIO_3$-induced oxidative stress mouse model. Shown are retinal function and anatomical changes of 8-week-old C57 mice treated with $NaIO_3$ or not after receiving intravitreal clopamide (CLO) or PBS. (**A**) Fundus photography revealed that no retinal damage occurred in $NaIO_3$-naïve mice. In contrast, in the $NaIO_3$-10 mg group, thiazide diuretics induced localized RPE layer damage (*white triangle arrows*). In the $NaIO_3$-30 mg group, the RPE layers in both eyes appeared "pebbled" (*white triangle arrows*). (**B**) OCT revealed the same trend as fundus photography in the $NaIO_3$-10 mg group, such that thiazide diuretics caused local uplift (*white triangle arrows*) in the RPE layer, with lesions extending to the outer nuclear and inner retinal layers (*white triangle arrows*) in the $NaIO_3$-30 mg group. *Scale bars*: 248 µm. (**C**) ERG showed that thiazide diuretics did not impair normal retinal function, but they could significantly reduce the b-wave amplitude of scotopic 0.01 and photopic 3.0 C57 mice treated with $NaIO_3$ (10 mg/kg). (**D**) Representative H&E staining of retinal morphology in different groups of C57 mice after receiving the intervention. (**E**) Representative TUNEL staining of retinal cell apoptosis in different groups of C57 mice after receiving the intervention; the *red signal* represents apoptosis. *Scale bars*: 50 µm. (**F**) ZO-1 staining of RPE flatmounts: $NaIO_3$-naïve mice did not exhibit abnormal changes in RPE layer tight junction proteins. After a 10-mg/kg $NaIO_3$ injection, multinucleated RPE cells were observed (*white triangle arrows*). On this basis, thiazide diuretics led to further damage to normal cell junctions (*white triangle arrows*). In $NaIO_3$-30 mg–treated mice, the RPE tight junction structure was completely destroyed, and thiazide diuretics induced more pronounced structural damage to RPE cells. *Scale bars*: 30 µm. Quantitative analysis data are expressed as mean + SD ($n = 3$). $^*P < 0.05$, $^{**}P < 0.01$, $^{***}P < 0.001$.

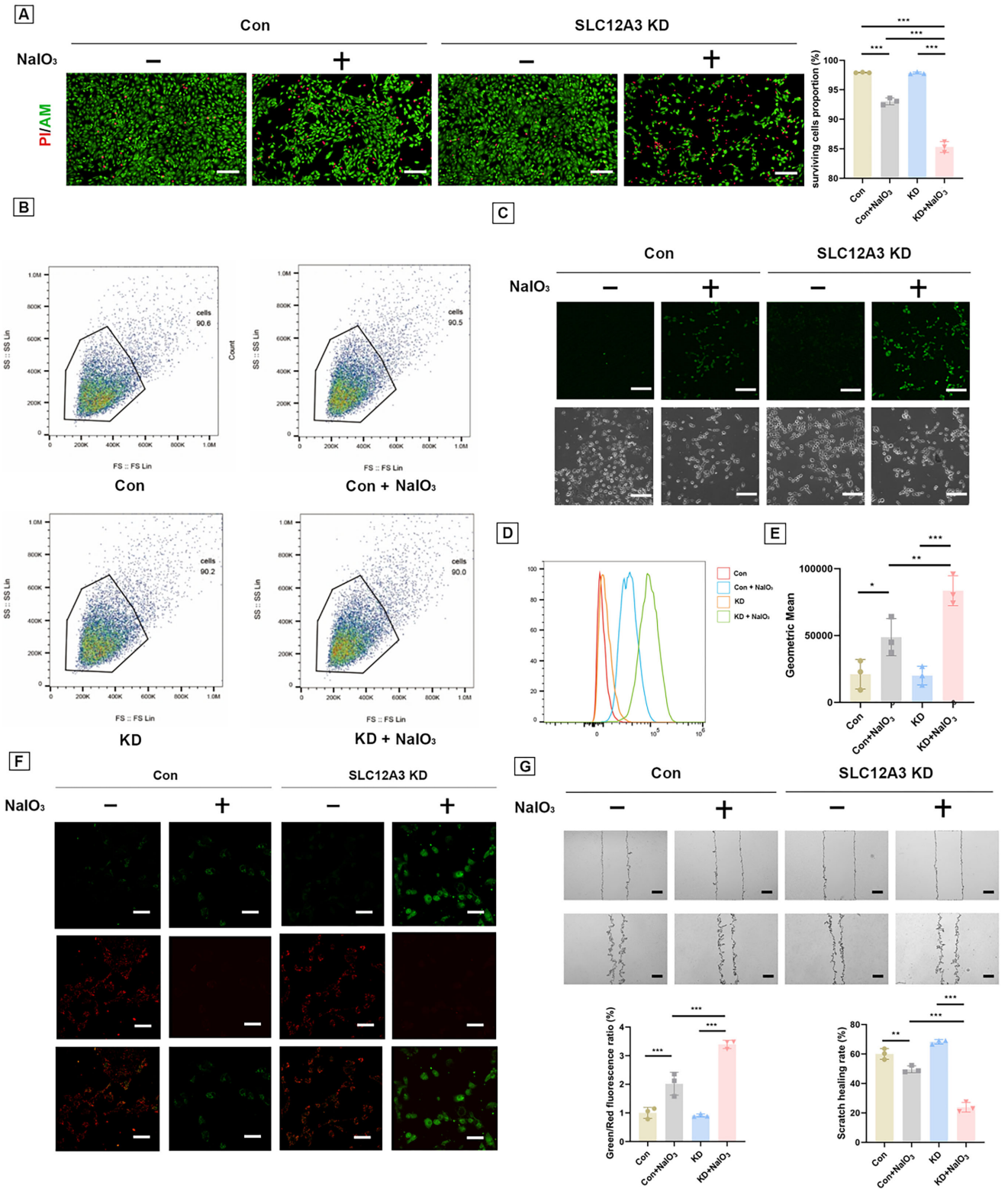

Figure 5. *SLC12A3* knockdown increased oxidative stress and RPE cell death when treated with $NaIO_3$. (**A**) Representative Live/Dead staining images and results of ARPE-19 with *SLC12A3* knockdown or without *SLC12A3* knockdown after receiving $NaIO_3$ intervention. *Scale bars*: 100 µm. (**B**) Gating strategies for flow cytometry. (**C–E**) Representative ROS staining and flow cytometry images and results of ARPE-19 with *SLC12A3* knockdown or without *SLC12A3* knockdown after receiving $NaIO_3$ intervention. *Scale bars*: 96 µm. (**F**) JC-1 staining and fluorescence intensity ratio (*green/red*). *Scale bars*: 50 µm. (**G**) Representative wound healing assay images and results of ARPE-19 with *SLC12A3* knockdown or without *SLC12A3* knockdown after receiving $NaIO_3$ intervention. *Scale bars*: 0.5 mm. Quantitative analysis data are expressed as mean + SD ($n = 3$). $^*P < 0.05$, $^{**}P < 0.01$, $^{***}P < 0.001$.

Investigative Ophthalmology & Visual Science

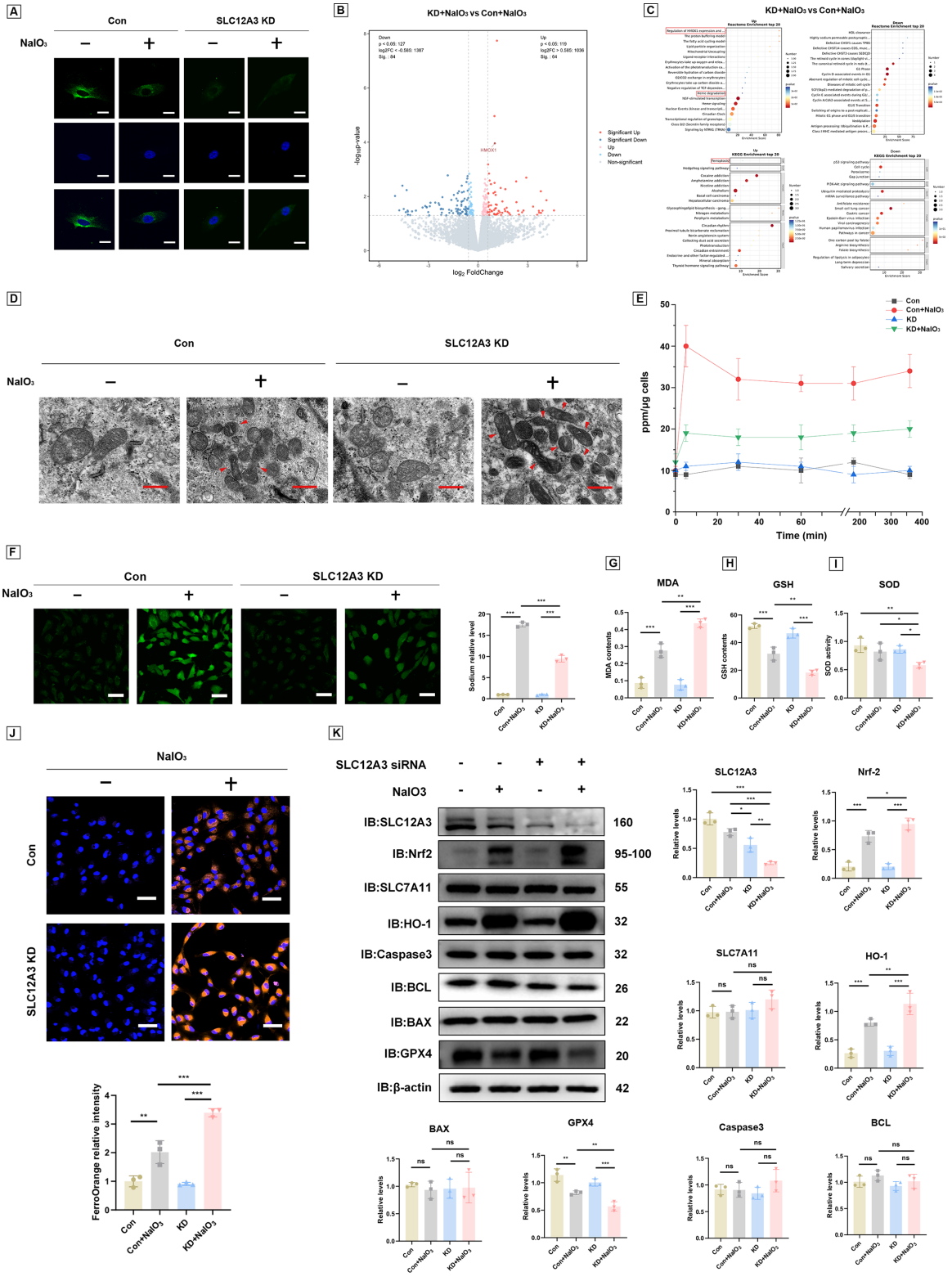

Figure 6. *SLC12A3* knockdown exacerbates ferroptosis in RPE cells against the background of oxidative stress. (**A**) *SLC12A3* was localized on the cell surface of ARPE-19 cells, with $NaIO_3$ treatment leading to downregulation of cell membrane *SLC12A3* expression. *Scale bars*: 20 μm. (**B**) A volcano plot showing 246 differentially expressed metabolites in the KD+$NaIO_3$ group compared to the Con+$NaIO_3$ group. (**C**) KEGG and Reactome enrichment analysis results. (**D**) TEM was used for ultrastructure analysis of mitochondria in ARPE-19 cells with or without *SLC12A3* knockdown and $NaIO_3$ intervention. *Scale bars*: 500 nm. (**E**) ICP showed Na^+ uptake in ARPE-19 cells of each group. (**F**) Sodium staining of ARPE-19 in each group. *Scale bars*: 100 μm. (**G**) MDA expression level measure results. (**H**) GSH expression level measure results. (**I**) SOD activity test results. (**J**) Ferrous ion staining for ARPE-19 in each group. *Scale bars*: 100 μm. (**K**) Representative western blot images showing changes in ferroptosis- and apoptosis-related molecular expression in ARPE-19 cells with or without *SLC12A3* knockdown following $NaIO_3$ treatment. Quantitative analysis data are expressed as mean + SD ($n = 3$). $^*P < 0.05$, $^{**}P < 0.01$, $^{***}P < 0.001$.

Investigative Ophthalmology & Visual Science

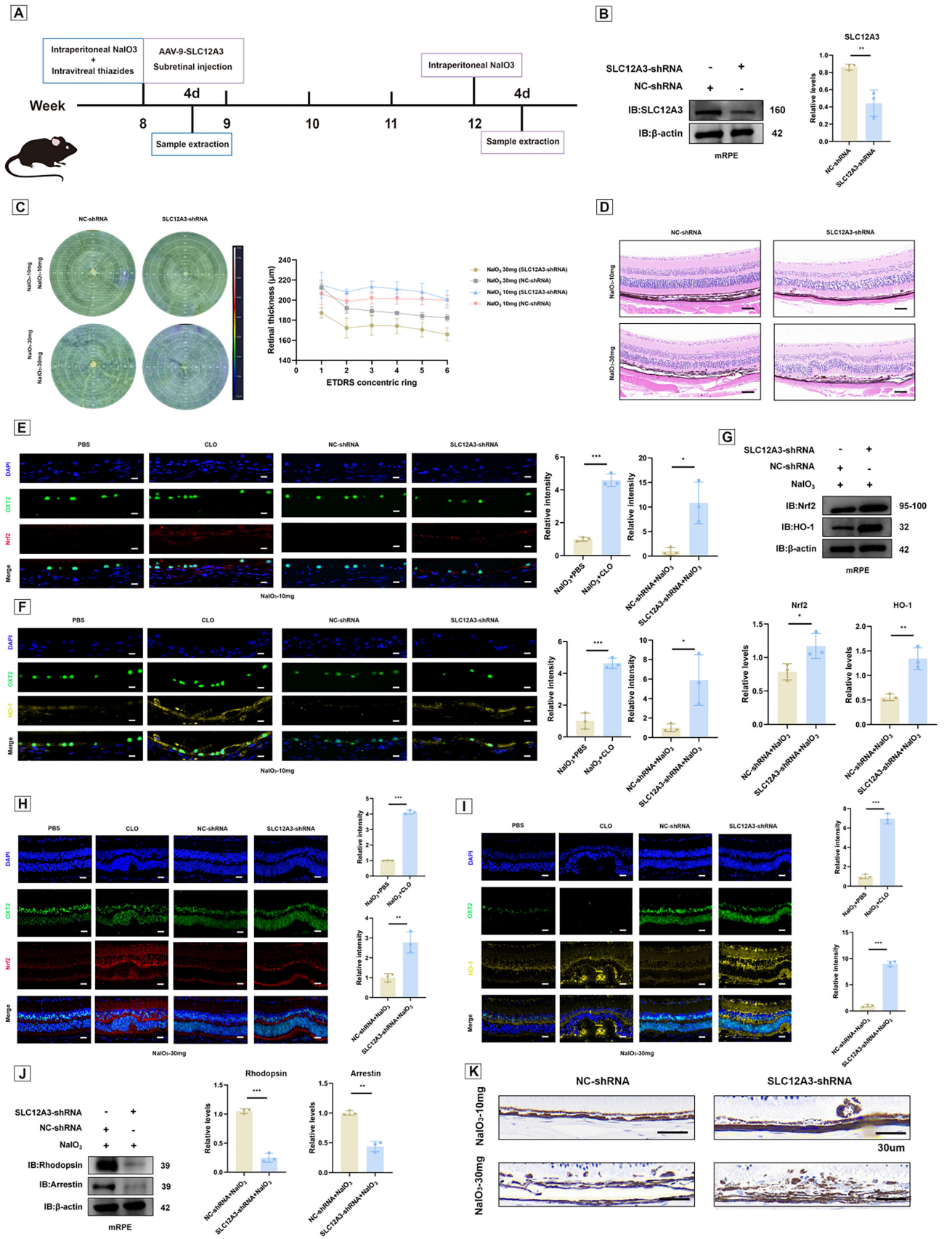

Figure 7. Knockdown of RPE *SLC12A3* in mice exacerbates retinal degeneration in the context of oxidative stress by modulating ferroptosis. (**A**) Schematic diagram of the intravitreal or subretinal injection process of a $NaIO_3$-induced AMD mouse model. (**B**) Representative western blot images and quantification of RPE *SLC12A3* expression in mice receiving AAV9 viral subretinal injection or no-loaded viral injection. (**C**) Representative images based on Early Treatment Diabetic Retinopathy Study concentric circles obtained by swept-source optical coherence tomography angiography ($n = 4$). (**D**) Representative H&E staining of retinal morphology in C57 mice undergoing subretinal injection

Investigative Ophthalmology & Visual Science

of AAV9 virus or no-loaded virus under oxidative stress. *Scale bars*: 50 µm. (**E**) Representative immunofluorescence images of Nrf2 of C57 mice RPE receiving AAV9 virus or no-loaded virus subretinal injection in the $NaIO_3$-10 mg group and their quantitative analysis. *Scale bars*: 20 µm. (**F**) Representative immunofluorescence images of HO-1 of C57 mice RPE receiving AAV9 virus or no-loaded virus subretinal injection in the $NaIO_3$-10 mg group and their quantitative analysis. *Scale bars*: 20 µm. (**G**) Representative western blotting images and results of Nrf2 and HO-1 expression based on RPE in oxidative stress mouse models ($NaIO_3$-10 mg) receiving AAV9 virus or no-loaded viral subretinal injection. (**H**) Representative immunofluorescence images of Nrf2 of C57 mice retina receiving AAV9 virus or no-loaded virus subretinal injection in the $NaIO_3$-30 mg group and their quantitative analysis. *Scale bars*: 20 µm. (**I**) Representative immunofluorescence images of HO-1 of C57 mice retina receiving AAV9 virus or no-loaded virus subretinal injection in the $NaIO_3$-30 mg group and their quantitative analysis. *Scale bars*: 20 µm. (J) Representative western blotting images and results of rhodopsin and arrestin expression based on RPE in oxidative stress mouse models ($NaIO_3$-30 mg) receiving AAV9 virus or no-loaded viral subretinal injection. (**K**) Representative Prussian blue staining of iron deposition (*black triangle arrows*) in RPE in C57 mice receiving subretinal injection of AAV9 virus or no-loaded virus under the background of oxidative stress. *Scale bars*: 30 µm. Quantitative analysis data are expressed as mean + SD ($n = 3$). $^*P < 0.05$, $^{**}P < 0.01$, $^{***}P < 0.001$.

localization of *SLC12A3*. The results demonstrated that the localization of *SLC12A3* in RPE cells was consistent with the distribution characteristics of membrane proteins (Fig. 6A). Immunofluorescence co-localization of RPE flat-mounts based on C57 mice was carried out to further clarify the expression location of *SLC12A3* to verify the results of the cell experiments above. The co-localization results with ZO-1 confirmed the presence of *SLC12A3* on the cell membrane of the RPE in C57 mice (Supplementary Fig. S6). Next, we conducted transcriptomic analysis using ARPE-19 cells to detect differential metabolites between the *SLC12A3* knockdown and non-knockdown groups under oxidative stress conditions. The volcano plot revealed 246 differentially expressed metabolites in the SLC12A3 knockdown (KD)+$NaIO_3$ group compared to the Control (CON)+$NaIO_3$ group (Fig. 6B). KEGG enrichment analysis indicated the involvement of ferroptosis-related pathways, and Reactome enrichment analysis highlighted heme degradation-related pathways, particularly those associated with heme oxygenase-1 (HO-1) (Fig. 6C). Notably, a comparison of the control versus Con+$NaIO_3$, knockdown versus KD+$NaIO_3$, and Con+$NaIO_3$ versus KD+$NaIO_3$ groups showed that the $NaIO_3$-induced oxidative stress models were closely linked to ferroptosis, regardless of whether *SLC12A3* was knocked down or not. Furthermore, 30 genes were commonly differentially expressed across these comparisons (Supplementary Fig. S10A). Gene Set Enrichment Analysis (GSEA) further suggested that *SLC12A3* knockdown may promote ferroptosis of ARPE-19 cells under oxidative stress conditions (Supplementary Fig. S10B). Using TEM, we observed unique morphological features of mitochondria in *SLC12A3* knockdown ARPE-19 cells treated with $NaIO_3$ for 24 hours, indicative of more pronounced ferroptosis, such as reduced mitochondrial volume, increased membrane density, and disruption of cristae, compared with the non-knockdown cells (Fig. 6D). By using ICP-MS to detect the dynamic changes in Na^+ uptake of ARPE-19 cells in different groups with or without $NaIO_3$ intervention, the results showed that Na^+ uptake in the Con+$NaIO_3$ group increased rapidly under oxidative stress. Knockdown of *SLC12A3* significantly reduced the Na^+ uptake induced by $NaIO_3$ intervention, but it remained higher than that in the control group. (Fig. 6E). SBFI AM staining revealed that $NaIO_3$ treatment elevated sodium ion concentrations in RPE cells, but the KD+$NaIO_3$ group exhibited significantly lower sodium ion levels than the Con+$NaIO_3$ group (Fig. 6F). Ferrostatin staining revealed that *SLC12A3* knockdown increased iron accumulation in ARPE-19 cells under oxidative stress conditions (Fig. 6J), but MDA analysis suggested increased levels of lipid peroxidation (Fig. 6G). Additionally, *SLC12A3* knockdown resulted in a decrease in GSH levels under oxidative stress (Fig. 6H) and downregulated SOD activity, reflecting diminished antioxidant capacity in RPE cells (Fig. 6I). To further investigate the impact of *SLC12A3* on cell death, we assessed ferroptosis- and apoptosis-related proteins based on transcriptomic data. After $NaIO_3$ treatment, the expression of nuclear factor erythroid 2-related factor 2 (Nrf2) and HO-1 was upregulated, whereas glutathione peroxidase 4 (GPX4) expression was downregulated. In contrast, *SLC12A3* knockdown RPE cells showed significantly higher Nrf2 and HO-1 levels and lower GPX4 expression and SOD activity compared to $NaIO_3$-treated cells without *SLC12A3* knockdown. However, no significant differences were observed in apoptosis-related proteins between the groups (Fig. 6K).

SLC12A3 Knockdown Exacerbates Oxidative Damage-Induced Retinal Degeneration by Regulating Nrf2/HO-1–Related Ferroptosis In Vivo

To corroborate the in vitro results, we injected the AAV9 virus into the subretinal space of 8-week-old mice (as shown in Fig. 7A) and confirmed successful knockdown of *SLC12A3* in the RPE layer after 4 weeks (Fig. 7B). OCT results revealed that, in the short term, *SLC12A3* knockdown in the RPE layer alone did not cause significant structural damage to the retina in normal mice (Supplementary Fig. S11). Following intraperitoneal $NaIO_3$ injection, retinal changes were assessed using OCT 4 days later. In the $NaIO_3$-10 mg group, localized damage to the RPE layer was observed after *SLC12A3* knockdown (Supplementary Fig. S12). In contrast, *SLC12A3* knockdown in the $NaIO_3$-30 mg group resulted in more severe retinal structural disarray (Supplementary Fig. S12), along with a significant decrease in retinal thickness (Fig. 7C). Histological analysis by H&E staining revealed significant hypertrophy, atrophy, and depigmentation of the local RPE layer in the $NaIO_3$-10 mg group with *SLC12A3* knockdown (Fig. 7D). Moreover, in the $NaIO_3$-30 mg group, *SLC12A3* knockdown caused extensive full-thickness retinal disruption (Fig. 7D). Immunofluorescence staining of HO-1 and Nrf2 in the retina, with orthodenticle homeobox 2 (OTX2) used to label the RPE cells for clear distinction from the choroidal layer, showed significant upregulation of these proteins in the retina of C57BL/6 mice subjected to oxidative stress with 10 mg $NaIO_3$ when *SLC12A3* was knocked down or its function inhibited (Figs. 7E; 7F). Western blot analysis further confirmed that the expression of Nrf2 and HO-1 in mice receiving AAV9 virus injection under oxidative stress ($NaIO_3$-10 mg) was significantly higher than that in the control group receiving no-loaded virus (Fig. 7G). Following intraperitoneal injection of 30 mg $NaIO_3$ under oxidative stress, OTX2 signal in the RPE layer was absent,

Investigative Ophthalmology & Visual Science

indicating severe destruction of the RPE cells. Although Nrf2 and HO-1 expression in the RPE layer could no longer be detected, their expression was significantly elevated in other layers of the retina in mice with *SLC12A3* knockdown or inhibition (Figs. 7H; 7I). Additionally, retinal damage to the photoreceptor cell layer was more pronounced in *SLC12A3*-knockdown mice. Western blot results showed significant downregulation of the rod and cone cell markers arrestin and rhodopsin in the retina of mice with *SLC12A3* knockdown or functional inhibition in the RPE layer (Fig. 7J).

Discussion

AMD is an essential retinal degenerative disease related to visual impairment in our aging society, imposing significant economic burdens globally.[41] Hypertension has been recognized as a risk factor that exacerbates the progression of AMD,[6,42] highlighting the importance of maintaining blood pressure within a reasonable range for potentially mitigating AMD risk. Research suggests that hypertension-induced choroidal perfusion abnormalities may significantly contribute to the pathogenesis of AMD.[43] Moreover, hypertension is known to accelerate elastin and collagen degenerative changes in Bruch's membrane, further elevating the risk of developing AMD.[44] In clinical practice, a wide array of antihypertensive medications, each with distinct mechanisms of action, are available and theoretically could offer benefits in alleviating the hypertension-induced pathological changes associated with AMD. However, observational studies examining the impact of these antihypertensive drugs on AMD have yielded mixed and often conflicting results. The precise effect of various antihypertensive drugs on AMD is still not completely clear.

In this study, we leveraged the drug targets of frequently used antihypertensive drugs and applied eQTLs of antihypertensive drug target gene proxies from the eQTLGen database—which contains the most comprehensive information on transcription factors in human blood samples—to serve as exposure variables, with AMD-related GWAS data as outcome variables. A potential association between *SLC12A3*, a genetic proxy for thiazide diuretics, and AMD was identified by SMR analysis screening. No potential associations were found between the genetic proxies of other antihypertensive drug targets and AMD. To substantiate the causal relationship between *SLC12A3* expression and AMD risk, traditional MR analysis was employed, corroborating the protective influence of *SLC12A3* against AMD. The positive control results confirm the causal effect of *SLC12A3* on the rise in SBP, confirming the reliability of our chosen genetic proxy for thiazide diuretic targets. Colocalization analysis also supported shared causal characteristics between *SLC12A3* and AMD. To augment the robustness of our genetic findings, we also conducted a cross-sectional analysis based on the UK Biobank and NHANES databases. Although the results of univariate analysis based on the NHANES suggested that the use of thiazide diuretics may be a protective factor for AMD, the results lacked precision due to the omission of covariates. We cannot ignore the influence of a large number of established risk factors for AMD (e.g., age, ethnicity, genetics, systemic conditions) on the overall outcome.[2,6,7] Consequently, the multiple regression analysis, which accounted for these risk factors, offered a more accurate reflection of the impact of thiazide diuretics on AMD risk, ultimately indicating a detrimental effect. Indeed, multiple regression analysis cannot completely exclude the influence of hypertension itself on AMD. Therefore, with sufficient inclusion of the population, further exclusion of hypertensive participants may better reflect the true results. In this study, the results based on UK Biobank model 3 ensured the stability of the final outcome.

Solute carriers (SLCs) constitute the largest family of transporters in the human body, and they crucial for maintaining cellular homeostasis through the regulation of solute exchange across lipid membranes.[45] Dysregulation of SLCs has been implicated in the pathogenesis of a myriad of chronic diseases, including hypertension, diabetes, chronic kidney disease, and various forms of cancer, by affecting key pathological mechanisms such as cell proliferation, migration, epithelial–mesenchymal transition, and angiogenesis.[46,47] *SLC12A3*, a vital member of the SLC12 branch, is broadly expressed across different human tissues and mediates the coupled movement of sodium and chloride ions, thus playing a significant role in cellular ion homeostasis.[48] Research by Gao et al.[49] highlighted the potential of *SLC12A3* to improve tumor prognosis through the enhancement of immune infiltration within the tumor microenvironment. However, the exploration of SLCs, particularly *SLC12A3*, in the context of AMD remains nascent. It is worth noting that there are clues from available studies, with results from a cohort of female teachers in California suggesting a higher risk of AMD in patients treated with diuretics compared with patients treated with other antihypertensive drugs.[13] Unfortunately, this study did not clearly distinguish between specific types of diuretics, but it still indirectly supports the original aims of this study to some extent. Another case–control study showed that thiazide diuretic intake was positively associated with severe vision loss and extensive choroidal neovascularization with severe subretinal hemorrhage.[14] The results of our genetic analysis suggest that the causal role of *SLC12A3* in AMD is not affected by AMD subtypes. However, the differences in the pathogenesis of the two subtypes of advanced AMD (dry/wet) cannot be ignored. Therefore, we hypothesized that the role of *SLC12A3* in AMD might be through a common initiation pathway in the pathogenesis of different AMD subtypes. Oxidative stress is considered to be a pivotal trigger point for the pathogenesis of AMD. Local excessive generation of ROS and the decrease of antioxidant capacity will lead to the apoptosis of RPE cells and the thickening of Bruch's membrane, resulting in the typical dry-AMD lesion feature, drusen.[50] Oxidative stress can also cause excessive secretion of pro-angiogenic factors including vascular endothelial growth factor (VEGF) and hypoxia inducible factor alpha (HIF-α) in RPE cells, leading to choroidal neovascularization,[51,52] which suggests that *SLC12A3* may be associated with oxidative stress. Physiological doses of IL-18 can inhibit the formation of neovascularization in wet AMD, and non-physiological doses of IL-18 can play a strong pro-inflammatory role, increase the infiltration of immune cells in the RPE layer, and reduce the viability of RPE cells.[53] The expression product of *SLC12A3*, NCC, has been confirmed to act as a receptor of IL-18 for cell signaling and affect a variety of cellular metabolic processes,[54,55] which may provide some inspiration for the next exploration of the mechanism of *SLC12A3* in AMD. In addition to focusing on the possible role of *SLC12A3* locally in the retina, it is impossible to ignore that *SLC12A3* is a gene that is highly expressed in the kidney, and mutations in *SLC12A3* cause Gitelman syndrome.[56] The metabolic profile of this disease is similar to that of thiazide diuretics and can cause ectopic calcification of the retina, leading to vision loss.[57] Retinal

Investigative Ophthalmology & Visual Science

calcification has been shown to contribute to the progression of AMD.[58]

Building on the above research foundation, this study employed in vitro and in vivo $NaIO_3$-mediated oxidative stress models to examine the effects of thiazide diuretics and the *SLC12A3* gene on AMD pathogenesis. $NaIO_3$ induces retinal oxidative stress and RPE abnormalities, mimicking the pathological features of AMD.[59] To observe the direct retinal impact of thiazide diuretics, we injected them into the vitreous body. Surprisingly, in both models, thiazide diuretics exacerbated death in $NaIO_3$-treated retinal and RPE cells, with control groups showing no damage to normal retinas. However, the phototoxicity of thiazide drugs is a well-recognized phenomenon based on current research.[60] Under different circumstances, such as long-term exposure to light at higher drug concentrations or in the presence of other predisposing factors, the phototoxicity of thiazides may pose a significant risk to patients with AMD. To cautiously rule out the influence of the phototoxicity of thiazide drugs on the pathological changes observed in our study, we set up a darkroom group under the same intervention conditions. The final results were consistent with those of the non-darkroom group. Combined with the results shown by the negative control group under normal light conditions, that intravitreal injection of thiazides alone did not cause RPE damage, these data strongly indicate that, under the specific concentration and experimental conditions of our study, the observed effects on the retina cannot be attributed to the phototoxicity of thiazides. Of note, the exclusion of phototoxicity under our specific conditions does not negate the possibility of relevant phototoxicity of thiazides in clinical scenarios or other experimental models. Future research should continue to explore the complex interactions related to the phototoxicity of thiazides, drug concentration, light exposure, and the progression of AMD. This will contribute to a more comprehensive understanding of the risks associated with the use of thiazides in AMD patients.

Molecular studies have revealed that *SLC12A3* downregulation significantly aggravates the destruction of mitochondrial membrane potential, promotes oxidative stress imbalance in RPE cells, and inhibits their viability. It is important to note that inhibiting *SLC12A3* function or directly knocking down *SLC12A3* has not been shown to damage the retina or RPE cells of normal mice, both in vitro and in vivo, suggesting that thiazides do not exhibit toxic effects on normal individuals. To elucidate the underlying mechanism of action of *SLC12A3* on RPE cell fate under oxidative stress, we conducted further molecular mechanism experiments. First, we confirmed that *SLC12A3* localized to the RPE cells in accordance with the distribution characteristics of membrane proteins. Second, transcriptomic analysis indicated that *SLC12A3* downregulation significantly increased HO-1 expression under oxidative stress. Enrichment and GSEA analyses further suggested that *SLC12A3* knockdown may promote ferroptosis of ARPE-19 cells in this context, a finding that was substantiated by TEM microstructure analysis. HO-1 is an enzyme responsible for oxidizing cellular heme to generate free ferrous iron, carbon monoxide, and biliverdin. The potent antioxidant activity of these metabolites helps to defend against ROS and provides cellular protection.[61] However, the accumulation of free ferrous iron can induce ferroptosis by contributing to intracellular iron overload.[62] Notably, previous studies have suggested that HO-1 overexpression may mediate RPE ferroptosis and promote AMD progression.[63] Based on these findings, we hypothesized that *SLC12A3* downregulation could promote ferroptosis of RPE cells by upregulating HO-1 expression. To test this hypothesis, we examined ferroptosis-related markers in each group of cells. *SLC12A3* knockdown significantly increased ferrous ion and MDA levels while decreasing GSH levels in RPE cells under oxidative stress. Additionally, HO-1 is known to be regulated by Nrf2,[63,64] and we also included Nrf2 and GPX4 (which is closely associated with GSH) in our western blot assays.[65] Western blot results confirmed that *SLC12A3* knockdown significantly increased Nrf2/HO-1 expression and decreased GPX4 expression under oxidative stress. Notably, *SLC12A3* knockdown exacerbated cell death under oxidative stress, independent of apoptosis. In vivo experiments in the mouse RPE layer further confirmed these findings through immunofluorescence co-localization. We observed that *SLC12A3* knockdown significantly increased Nrf2/HO-1 expression in the RPE layer in a mouse model of oxidative stress, with the harmful effects being amplified by increasing $NaIO_3$ dose, leading to more severe damage to cones and rods. However, our results did not find an association between *SLC12A3* and *SLC7A11* in regulating the Nrf2/HO-1 pathway, although *SLC7A11* has been reported to slow the progression of neovascular AMD by inhibiting ferroptosis in RPE cells.[66] Because *SLC12A3* plays a role in regulating the sodium balance inside and outside the cells, we also measured sodium uptake and the changes in sodium ion concentration in each group of cells. Interestingly, we found that $NaIO_3$ increased sodium uptake in normal RPE cells and significantly elevated intracellular sodium ion concentration. Based on this finding, knockout of *SLC12A3* significantly reduced sodium ion uptake and intracellular sodium ion concentrations in RPE cells. However, in the absence of oxidative stress, the knockdown of *SLC12A3* had no impact on the intracellular sodium level. Sodium is a crucial component for maintaining plasma membrane potential and mitochondrial inner membrane potential, both essential for cellular energy balance.[67] Cytosolic sodium dynamics are tightly coupled with mitochondrial Na^+, and alterations in sodium ion concentrations can directly affect mitochondrial activity and energy production.[68] Although the relationship between intracellular Na^+ and oxidative stress remains largely unexplored, we hypothesize that the sodium concentration increase in RPE cells under oxidative stress could represent a defensive cellular response. The reduction in sodium uptake due to *SLC12A3* knockdown may further impair mitochondrial function, warranting additional experimental investigation.

This study proposed that thiazide diuretics may potentially affect the occurrence and development of AMD. Genetic analysis based on GWAS data and cross-sectional clinical studies based on the UK Biobank and NHANES can circumvent ethical issues that may be raised by human drug trials. As a key component of the genetic analysis methodology, MR analysis allows for minimization of confounding biases, simulating the reliability of randomized controlled trials. In addition, the IVs used in our genetic analysis were extracted from the latest GWAS database available at present. The sample included in the cross-sectional study covered all participants with AMD information in the UK Biobank and NHANES database, and the fact that the participants represent multi-ethnic populations compensates for the genetic analysis using samples from only European populations. The in vitro and in vivo mechanism studies further validate the accuracy and scientific rigor of the genetic analysis and clin-

Investigative Ophthalmology & Visual Science

ical research findings. It is worth noting that the SMR analysis results did not find a potential association between other antihypertensive drug targets and AMD; therefore, we do not deny the potentially positive effect of antihypertensive treatment on improving AMD. Our findings only suggest that patients with AMD should exercise caution when selecting thiazide diuretics among antihypertensive options. Despite these insights, our study faces several limitations. The GWAS data from blood tissues, although representative, may not capture the nuances of AMD pathogenesis as precisely as data from fundus tissues, such as the RPE layer and choroid, which are currently lacking in GWAS databases. In the SMR analysis, the association between *SLC12A3* and dry AMD was statistically significant, but the results of the colocalization analysis were moderate, which does not entirely eliminate the possibility of false-positive findings regarding the risk of dry AMD from thiazide diuretics. The uneven distribution between cases and controls within the GWAS dataset, particularly regarding the proportion of AMD subtypes (dry AMD and wet AMD), presents difficulties in achieving sufficient statistical power to accurately interpret the results. This shortcoming is an inherent issue in the current datasets. There may be additional covariates affecting the outcomes of multivariate regression models that were not considered in this study. Also, because the data from participants included in the cross-sectional study could not distinguish between diverse AMD subtypes, subgroup outcomes in the genetic analysis could not be further validated via cross-sectional study. Finally, although the $NaIO_3$-induced oxidative stress model is able to mimic some of the key pathological features of AMD, it may not be able to fully replicate all the complexities of human AMD, such as inflammation, genetic background, and other factors.

Conclusions

This study is a groundbreaking exploration of the association between antihypertensive medications and AMD that used multiple genetic analysis methods in conjunction with observational clinical studies based on the UK Biobank and NHANES. In vivo and in vitro experiments showed

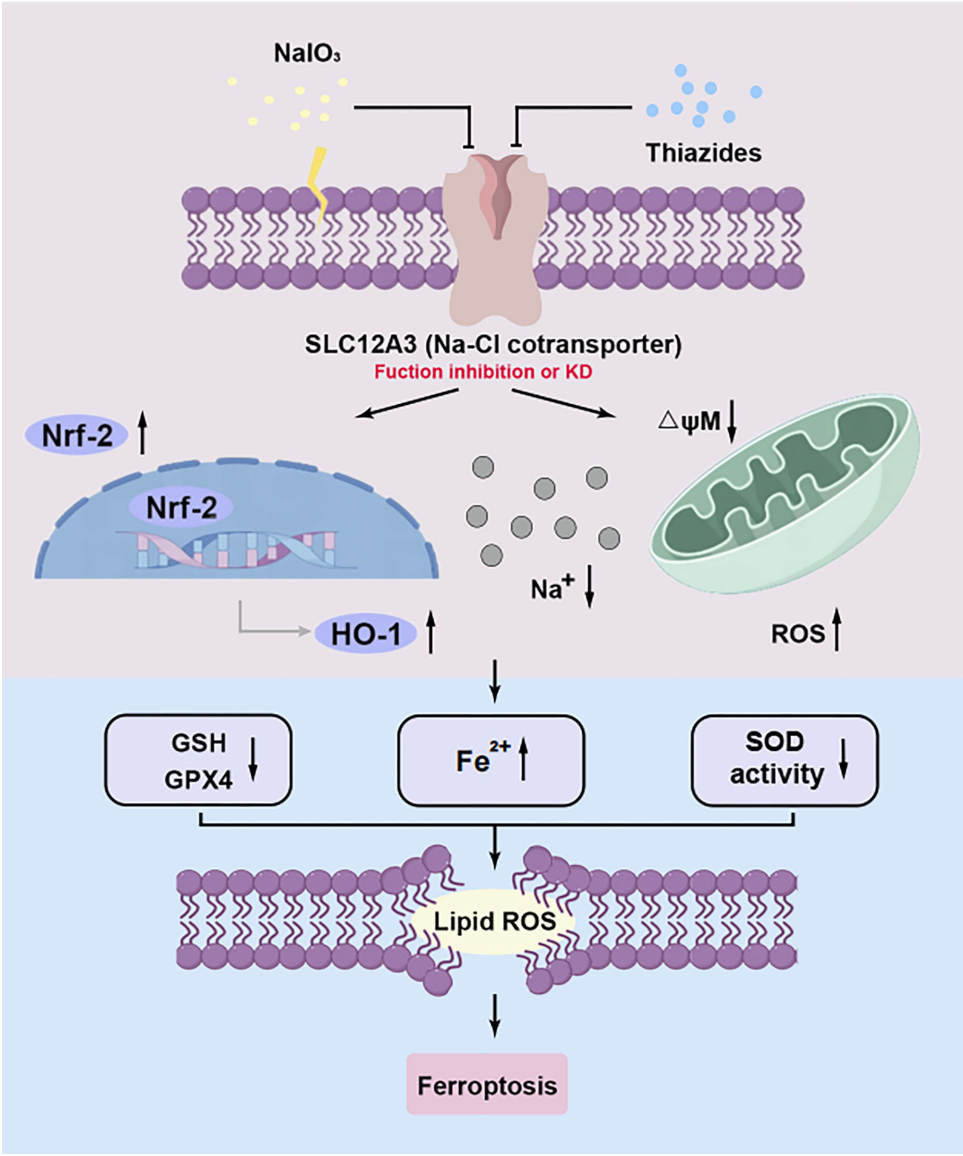

Figure 8. Schematic diagram of the molecular mechanisms by which thiazides exacerbate the risk and progression of AMD.

that thiazide diuretics worsened retinal damage in AMD mouse models, and *SLC12A3* knockdown disrupted the balance of oxidative stress in RPE cells. Further molecular mechanism experiments showed that *SLC12A3* knockdown promoted retinal degeneration by regulating RPE ferroptosis through activation of the Nrf2/HO-1 pathway (Fig. 8). Our results underscore a notable causal association between thiazide diuretic use and AMD risk. However, larger scale genetic engineering trials, expansive multicenter clinical trials, and in-depth mechanistic extension trials are imperative to enhance the accuracy and validity of our findings.

Acknowledgments

The authors thank the eQTLGen Consortium, FinnGen project, UK Biobank, NHANES, and IEU OpenGWAS project for publicly providing all the data for this study. We thank Zhang Jing (Second Department of Infectious Disease, Shanghai Fifth People's Hospital, Fudan University) for his work on the NHANES database. His outstanding work on the nhanesR package and webpage makes it easier for us to explore NHANES database. We also express our gratitude for the assistance provided by the scientific research drawing tool within the "Roche Club" platform, developed by Roche. Roche Club is a dedicated research-enabling platform by Roche, which offers a suite of tools, including the one we used for creating the figures in this manuscript. In addition, we are thankful for the support from PowerPoint and WPS software in the production of the images.

Supported by grants from the National Natural Science Foundation of China (82471089), Xi'an Science and Technology Plan Project (2024JH-YLYB-0324), Shaanxi Province Traditional Chinese Medicine Research Project (SZY-KJCYC-2023-028), Air Force Military Medical University Clinical Research Program (2022LC2227), Tangdu Hospital Discipline Innovation Development Plan (2021LCYJ019), and the "Rapid Response" scientific research topic of Air Force Military Medical University.

Author Contributions: C.C., Original draft writing; C.C. and J.H., data extraction; C.C., T.X., H.Z., and Y.L., data analysis; J.H., C.C., L.T., and X.Y., idea; C.C., H.Z., T.X., and L.C., scheme design; C.C., C.F., D.W., X.W., S.L., Y.C., Y.L., and X.W., graphical design; J.H., L.T., L.S. and X.Y., manuscript review.

Disclosure: **C. Chen**, None; **T. Xie**, None; **H. Zhang**, None; **L. Chang**, None; **Y. Lan**, None; **C. Fan**, None; **D. Wei**, None; **X. Wang**, None; **S. Liu**, None; **Y. Chen**, None; **Y. Chen**, None; **X. Wang**, None; **X. Yan**, None; **L. Shang**, None; **L. Tao**, None; **J. Han**, None

References

1. Guymer RH, Campbell TG. Age-related macular degeneration. *Lancet.* 2023;401(10386):1459–1472.
2. Wong WL, Su X, Li X, et al. Global prevalence of age-related macular degeneration and disease burden projection for 2020 and 2040: a systematic review and meta-analysis. *Lancet Glob Health.* 2014;2(2):e106–e116.
3. Ferris FL, 3rd, Wilkinson CP, Bird A, et al. Clinical classification of age-related macular degeneration. *Ophthalmology.* 2013;120(4):844–851.
4. Age-Related Eye Disease Study Research Group. A randomized, placebo-controlled, clinical trial of high-dose supplementation with vitamins C and E, beta carotene, and zinc for age-related macular degeneration and vision loss: AREDS report no. 8. *Arch Ophthalmol.* 2001;119(10):1417–1436.
5. Jager RD, Mieler WF, Miller JW. Age-related macular degeneration. *N Engl J Med.* 2008;358(24):2606–2617.
6. Age-Related Eye Disease Study Research Group. Risk factors associated with age-related macular degeneration. A case-control study in the age-related eye disease study: Age-Related Eye Disease Study Report Number 3. *Ophthalmology.* 2000;107(12):2224–2232.
7. Cook HL, Patel PJ, Tufail A. Age-related macular degeneration: diagnosis and management. *Br Med Bull.* 2008;85:127–149.
8. Yun C, Ahn J, Kim M, Hwang SY, Kim SW, Oh J. Ocular perfusion pressure and choroidal thickness in early age-related macular degeneration patients with reticular pseudodrusen. *Invest Ophthalmol Vis Sci.* 2016;57(15):6604–6609.
9. Grimes KR, Aloney A, Skondra D, Chhablani J. Effects of systemic drugs on the development and progression of age-related macular degeneration. *Surv Ophthalmol.* 2023;68(3):332–346.
10. Klein R, Deng Y, Klein BE, et al. Cardiovascular disease, its risk factors and treatment, and age-related macular degeneration: Women's Health Initiative Sight Exam ancillary study. *Am J Ophthalmol.* 2007;143(3):473–483.
11. Klein R, Myers CE, Klein BE. Vasodilators, blood pressure-lowering medications, and age-related macular degeneration: the Beaver Dam Eye Study. *Ophthalmology.* 2014;121(8):1604–1611.
12. van Leeuwen R, Tomany SC, Wang JJ, et al. Is medication use associated with the incidence of early age-related maculopathy? Pooled findings from 3 continents. *Ophthalmology.* 2004;111(6):1169–1175.
13. Xu X, Ritz B, Coleman A, et al. Hypertension, antihypertensive medications use and risk of age-related macular degeneration in California Teachers Cohort. *J Hum Hypertens.* 2020;34(8):568–576.
14. de La Marnierre E, Guigon B, Quaranta M, Mauget-Faÿsse M. [Phototoxic drugs and age-related maculopathy]. *J Fr Ophtalmol.* 2003;26(6):596–601.
15. Smith GD, Ebrahim S. 'Mendelian randomization': can genetic epidemiology contribute to understanding environmental determinants of disease? *Int J Epidemiol.* 2003;32(1):1–22.
16. Lawlor DA, Harbord RM, Sterne JA, Timpson N, Davey Smith G. Mendelian randomization: using genes as instruments for making causal inferences in epidemiology. *Stat Med.* 2008;27(8):1133–1163.
17. Burgess S, Small DS, Thompson SG. A review of instrumental variable estimators for Mendelian randomization. *Stat Methods Med Res.* 2017;26(5):2333–2355.
18. Lin J, Zhou J, Xu Y. Potential drug targets for multiple sclerosis identified through Mendelian randomization analysis. *Brain.* 2023;146(8):3364–3372.
19. Wang J, Iacovelli J, Spencer C, Saint-Geniez M. Direct effect of sodium iodate on neurosensory retina. *Invest Ophthalmol Vis Sci.* 2014;55(3):1941–1953.
20. Chen C, Lan Y, Wang Z, Yan W, Yan X, Han J. Causal effects of diabetic retinopathy on depression, anxiety and bipolar disorder in the European population: a Mendelian randomization study. *J Endocrinol Invest.* 2024;47(3):585–592.
21. Võsa U, Claringbould A, Westra HJ, et al. Large-scale *cis*- and *trans*-eQTL analyses identify thousands of genetic loci and polygenic scores that regulate blood gene expression. *Nat Genet.* 2021;53(9):1300–1310.
22. Xue CC, Li H, Yu M, et al. Omega-3 fatty acids as protective factors for age-related macular degeneration: prospective cohort and Mendelian randomization analyses. *Ophthalmology.* 2025;132(5):598–609.
23. Winkler TW, Grassmann F, Brandl C, et al. Genome-wide association meta-analysis for early age-related macular degeneration highlights novel loci and insights for advanced disease. *BMC Med Genomics.* 2020;13(1):120.

24. Evangelou E, Warren HR, Mosen-Ansorena D, et al. Genetic analysis of over 1 million people identifies 535 new loci associated with blood pressure traits. *Nat Genet.* 2018;50(10):1412–1425.
25. Bycroft C, Freeman C, Petkova D, et al. The UK Biobank resource with deep phenotyping and genomic data. *Nature.* 2018;562(7726):203–209.
26. Chen C, Zhang H, Lan Y, et al. Statins as a risk factor for diabetic retinopathy: a Mendelian randomization and cross-sectional observational study. *J Transl Med.* 2024;22(1): 298.
27. Huang W, Xiao J, Ji J, Chen L. Association of lipid-lowering drugs with COVID-19 outcomes from a Mendelian randomization study. *eLife.* 2021;10:e73873.
28. Skrivankova VW, Richmond RC, Woolf BAR, et al. Strengthening the reporting of observational studies in epidemiology using Mendelian randomization: the Strobe-MR Statement. *JAMA.* 2021;326(16):1614–1621.
29. Burgess S, Thompson SG. Avoiding bias from weak instruments in Mendelian randomization studies. *Int J Epidemiol.* 2011;40(3):755–764.
30. Wang Z, Lu J, Hu J. Association between antihypertensive drugs and hepatocellular carcinoma: a trans-ancestry and drug-target Mendelian randomization study. *Liver Int.* 2023;43(6):1320–1331.
31. Foley CN, Staley JR, Breen PG, et al. A fast and efficient colocalization algorithm for identifying shared genetic risk factors across multiple traits. *Nat Commun.* 2021;12(1):764.
32. Chen J, Xu F, Ruan X, et al. Therapeutic targets for inflammatory bowel disease: proteome-wide Mendelian randomization and colocalization analyses. *eBioMedicine.* 2023;89:104494.
33. Chauquet S, Zhu Z, O'Donovan MC, Walters JTR, Wray NR, Shah S. Association of antihypertensive drug target genes with psychiatric disorders: a Mendelian randomization study. *JAMA Psychiatry.* 2021;78(6):623–631.
34. Bowden J, Del Greco MF, Minelli C, et al. Improving the accuracy of two-sample summary-data Mendelian randomization: moving beyond the NOME assumption. *Int J Epidemiol.* 2019;48(3):728–742.
35. Burgess S, Thompson SG. Interpreting findings from Mendelian randomization using the MR-Egger method. *Eur J Epidemiol.* 2017;32(5):377–389.
36. Hemani G, Bowden J, Davey Smith G. Evaluating the potential role of pleiotropy in Mendelian randomization studies. *Hum Mol Genet.* 2018;27(R2):R195–R208.
37. Bowden J, Holmes MV. Meta-analysis and Mendelian randomization: a review. *Res Syn Methods.* 2019;10(4):486–496.
38. Emdin CA, Khera AV, Kathiresan S. Mendelian randomization. *JAMA.* 2017;318(19):1925–1926.
39. Verbanck M, Chen CY, Neale B, Do R. Detection of widespread horizontal pleiotropy in causal relationships inferred from Mendelian randomization between complex traits and diseases. *Nat Genet.* 2018;50(5):693–698.
40. Armstrong RA. When to use the Bonferroni correction. *Ophthalmic Physiol Opt.* 2014;34(5):502–508.
41. GBD 2019 Blindness and Vision Impairment Collaborators; Vision Loss Expert Group of the Global Burden of Disease Study. Causes of blindness and vision impairment in 2020 and trends over 30 years, and prevalence of avoidable blindness in relation to VISION 2020: the Right to Sight: an analysis for the Global Burden of Disease Study. *Lancet Glob Health.* 2021;9(2):e144–e160.
42. Hyman L, Schachat AP, He Q, Leske MC. Hypertension, cardiovascular disease, and age-related macular degeneration. Age-Related Macular Degeneration Risk Factors Study Group. *Arch Ophthalmol.* 2000;118(3):351–358.
43. Boltz A, Luksch A, Wimpissinger B, et al. Choroidal blood flow and progression of age-related macular degeneration in the fellow eye in patients with unilateral choroidal neovascularization. *Invest Ophthalmol Vis Sci.* 2010;51(8):4220–4225.
44. Cougnard-Grégoire A, Delyfer MN, Korobelnik JF, et al. Long-term blood pressure and age-related macular degeneration: the ALIENOR study. *Invest Ophthalmol Vis Sci.* 2013;54(3):1905–1912.
45. Pizzagalli MD, Bensimon A, Superti-Furga G. A guide to plasma membrane solute carrier proteins. *FEBS J.* 2021;288(9):2784–2835.
46. Hediger MA, Romero MF, Peng JB, Rolfs A, Takanaga H, Bruford EA. The ABCs of solute carriers: physiological, pathological and therapeutic implications of human membrane transport proteinsIntroduction. *Pflügers Archiv.* 2004;447(5):465–468.
47. Rashid K, Ahmad A, Liang L, Liu M, Cui Y, Liu T. Solute carriers as potential oncodrivers or suppressors: their key functions in malignant tumor formation. *Drug Discov Today.* 2021;26(7):1689–1701.
48. Meor Azlan NF, Zhang J. Role of the cation-chloride-cotransporters in cardiovascular disease. *Cells.* 2020;9(10):2293.
49. Gao Q, Ye X, Li F. SLC12A3: a novel prognostic biomarker of clear cell renal cell carcinoma. *Altern Ther Health Med.* 2024;30(9):286–293.
50. Deng Y, Qiao L, Du M, et al. Age-related macular degeneration: epidemiology, genetics, pathophysiology, diagnosis, and targeted therapy. *Genes Dis.* 2022;9(1):62–79.
51. Babapoor-Farrokhran S, Qin Y, Flores-Bellver M, et al. Pathologic vs. protective roles of hypoxia-inducible factor 1 in RPE and photoreceptors in wet vs. dry age-related macular degeneration. *Proc Natl Acad Sci USA.* 2023;120(50):e2302845120.
52. Sun RX, Zhu HJ, Zhang YR, et al. ALKBH5 causes retinal pigment epithelium anomalies and choroidal neovascularization in age-related macular degeneration via the AKT/mTOR pathway. *Cell Rep.* 2023;42(7):112779.
53. Campbell M, Doyle S, Humphries P. IL-18: A new player in immunotherapy for age-related macular degeneration? *Expert Rev Clin Immunol.* 2014;10(10):1273–1275.
54. Wang J, Sun C, Gerdes N, et al. Interleukin 18 function in atherosclerosis is mediated by the interleukin 18 receptor and the Na-Cl co-transporter. *Nat Med.* 2015;21(7):820–826.
55. Zhang X, Luo S, Wang M, et al. Differential IL18 signaling via IL18 receptor and Na-Cl co-transporter discriminating thermogenesis and glucose metabolism regulation. *Nat Commun.* 2022;13(1):7582.
56. Simon DB, Nelson-Williams C, Bia MJ, et al. Gitelman's variant of Bartter's syndrome, inherited hypokalaemic alkalosis, is caused by mutations in the thiazide-sensitive Na-Cl cotransporter. *Nat Genet.* 1996;12(1):24–30.
57. Ham Y, Mack H, Colville D, Harraka P, Savige J. Gitelman syndrome and ectopic calcification in the retina and joints. *Clin Kidney J.* 2021;14(9):2023–2028.
58. Tan ACS, Pilgrim MG, Fearn S, et al. Calcified nodules in retinal drusen are associated with disease progression in age-related macular degeneration. *Sci Transl Med.* 2018;10(466):eaat4544.
59. Ma X, Chen H, Jian S, et al. DAPL1 deficiency in mice impairs antioxidant defenses in the RPE and leads to retinal degeneration with AMD-like features. *Redox Biol.* 2023;62: 102675.
60. Karkoszka M, Rok J, Rzepka Z, Banach K, Kowalska J, Wrześniok D. Phototoxic reactions inducted by hydrochlorothiazide and furosemide in normal skin cells—

in vitro studies on melanocytes and fibroblasts. *Int J Mol Sci.* 2024;25(3):1432.

61. Wei D, Qu C, Zhao N, et al. The significance of precisely regulating heme oxygenase-1 expression: Another avenue for treating age-related ocular disease? *Ageing Res Rev.* 2024;97:102308.
62. Li R, Wei R, Liu C, et al. Heme oxygenase 1-mediated ferroptosis in Kupffer cells initiates liver injury during heat stroke. *Acta Pharm Sin B.* 2024;14(9):3983–4000.
63. Tang Z, Ju Y, Dai X, et al. HO-1-mediated ferroptosis as a target for protection against retinal pigment epithelium degeneration. *Redox Biol.* 2021;43:101971.
64. Fang X, Wang H, Han D, et al. Ferroptosis as a target for protection against cardiomyopathy. *Proc Natl Acad Sci USA.* 2019;116(7):2672–2680.
65. Zhang W, Dai J, Hou G, et al. SMURF2 predisposes cancer cell toward ferroptosis in GPX4-independent manners by promoting GSTP1 degradation. *Mol Cell.* 2023;83(23):4352–4369.e8.
66. Zhao X, Gao M, Liang J, et al. SLC7A11 reduces laser-induced choroidal neovascularization by inhibiting RPE ferroptosis and VEGF production. *Front Cell Dev Biol.* 2021;9:639851.
67. Hernansanz-Agustín P, Morales-Vidal C, Calvo E, et al. A transmitochondrial sodium gradient controls membrane potential in mammalian mitochondria. *Cell.* 2024;187(23):6599–6613.e21.
68. Borriello G, Buonincontri V, de Donato A, et al. The interplay between sodium/glucose cotransporter type 2 and mitochondrial ionic environment. *Mitochondrion.* 2024;76:101878.

Investigative Ophthalmology & Visual Science